東京大学 大学院新領域創成科学研究科
基盤科学研究系
先端エネルギー工学専攻

平成 23 年度

修士論文

Automated Impedance Matching System for Robust Wireless Power Transfer via Magnetic Resonance Coupling

－　自動インピーダンス整合による磁界共振結合ワイヤレス電力伝送システムのロバスト化　－

2012 年 2 月提出
指導教員　堀　洋一　教授

47106069　Beh Teck Chuan

Abstract

Recently, a highly efficiency mid-range wireless power transfer technology using electromagnetic resonance coupling was proposed, and has received much attention due to its practical range and efficiency. The resonance frequency of the resonators changes as the gap between the resonators change. However, when this technology is applied in the MHz range, the usable frequency is bounded by the Industrial, Scientific, Medical band. Therefore, to achieve maximum power transmission efficiency, the resonance frequency has to be fixed within the ISM band. In this paper, an automated Impedance Matching (IM) system is proposed to maintain maximum efficiency by matching the resonators. This includes achieving resonance by matching the resonance frequency of the resonator pair to that of the power source, and by making a sharper peak at the resonance frequency. The simulation and experiments verify that the IM circuit can induce resonation for different air gaps, improving the power efficiency. The IM circuit is also automated, to make the system more flexible towards varying air gaps. A high speed matching algorithm based on the Golden Section Search optimization technique was proposed to improve the matching speed, and study the maximum achievable matching speed of an IM system that automates by observing and minimizing the reflected wave at the transmitting side of the system.

Keywords: Automation, Impedance matching, Magnetic Resonance Coupling, Efficiency, Golden Section Search, Best-Step Steepest Descent Search, Wireless Power Transfer

Table of Contents

Chapter 1 Introduction

This research studies the Wireless Power Transfer (WPT) system via Magnetic Resonance Coupling (MRC) in the MHz range. In this paper, an automated Impedance Matching (IM) system is proposed to maximize the efficiency at varying gap-sizes, making the system more robust. This paper briefly explains the background of WPT via MRC and the theories of MRC before going into detail of the proposed IM system. Several studies were made through simulations and experiments to study the proposed system before the observations were concluded and future topics are suggested.

1.1 Research Background

Nowadays, with the development of mobile appliances and the recent boom of Electric Vehicles (EV), the need for a technique to wirelessly charge these appliances has increased. [1][2].A convenient, safe and efficiency way to charge these devices can increase the mobility, improve safety, as well as indirectly reducing the cost. This means that a WPT system does not only mean cutting the cord between the power and the appliance, it will revolutionize how the appliances are used, just like how the invention of the mobile phone drastically changed how telephones are used in the communications industry. Some of the examples where a practical WPT system will bring a revolution to are as below.

- Charging EVs : WPT is essential to the spread of EV usage as it provides a safe and convenient way to charge EVs. An EV has to be charged more often than a regular gasoline engine car as its energy storage medium (battery or capacitor) has a much lower energy density compared to petroleum. Therefore, a WPT system can be used in the automatic charging system which makes the charging of EVs more convenient. Also, as the process of plugging the power cord into the socket will be unnecessary, the danger of being electrocuted due to the wear and tears of an old cord, or rain will be avoided, making the charging process safer. For example, the power transmitting antenna can be placed in the car park, and the receiving antenna can be placed in the car. This enables the EV to be charged wirelessly just be being in the parking box. To achieve this, the wireless power transfer system must satisfy these three conditions: High efficiency, large air gaps, and high power. Our team in Hori-Fujimoto Laboratory are working on a wirelessly charge capacitor EV, which will be charged as it passes through a charging resonator, starting from a stationary spot such as a parking lot, to eventually moving pick-ups. Fig 1.1 shows an example of wireless EV charging done with the magnetic resonance coupling technology.
-

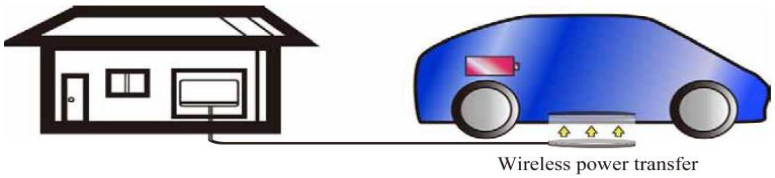

Fig 1.1 An example of WPT application. Charging EVs

- Charging mobile appliances such as laptops and mobile phones : While these appliances are already mobile by nature, their ranges are still limited by the battery which supplies their power. A WPT system will allow these appliances to be constantly charged as long as they are in a "charging area". This will not only increase the range of these appliances, but it will also eventually decrease the size of their battery, further increasing its mobility and decreasing its cost. Our team here also works on projects like the "wireless house" which allows WPT to every appliance within the building.
- Charging electrical appliances : This include wireless charging to bigger appliances such as television sets and electrical blankets, which can potentially make a previously stationary thing mobile, to smaller electrical appliances such as medical implants. The latter is particularly useful as it will allow the medical implants to be charged constantly without external connections, making it much less intrusive and safe to use.
- Other uses : WPT also plays a big role in precision engineering and clean rooms as it can reduce the contact surface between the equipments. This is important to reduce the dust created through friction if these equipments are moving.

As a result, the WPT field has enjoyed great attention and progress. Recent researches include WPT for small electronic devices such as mobile appliances [3][4], and medical implants [5] – [7] and bigger, high power devices such as EV [8][9]. The examples above shows that there are many usages for WPT, and it harbors a huge potential. This acts as the main source of motivation for this research.

1.1.1 Wireless Power Transfer (WPT) via Magnetic Resonance Coupling (MRC)

Presently, there are several types of WPT technologies such as the microwave power transfer, laser power transfer, electromagnetic induction and recently, the MRC. The first two WPT technologies are classified as radiative WPT systems, where the power is transferred as electromagnetic waves. They have extremely large range (several km), but generally has a low power transfer efficiency as the waves diverges and the receptors have a low efficiency. On the other hand, the last two WPT technologies are non-radiative, meaning the power is transferred as electromagnetic fields. While the electromagnetic fields cannot travel far, the efficiency of the WPT system is high as the receiver will potentially be able to pick up all the transferred energy, hence

having a higher efficiency.

Currently, the most common WPT technology now is the electromagnetic induction method, which is a very efficiency non-radiative WPT. However, it generally has a small air-gap at several centimeters, and recently improved to approximately 10cm by increasing its frequency to 20~40 kHz. Furthermore, its efficiency drops severely when there is a misalignment between its transmitting and receiving coils, even when the misalignment is only several centimeters.

Recently, a highly efficient mid-range WPT technology that transfers the energy via magnetic resonance coupling (MRC) was rediscovered and proposed [10] – [12], and has received much attention due to its high efficiency and practical mid-range [13] – [15]. It has an efficiency of approximately 90% within 1 meter, and 45% at 2 meters [10][11]. The basic characteristics of MRC that are presently known include:

- The power is transferred via the couplings of resonating magnetic fields
- In the strongly coupled regime, a high power transfer efficiency can be achieved even when the coupling coefficient, k, is small (k<0.1).
- At high frequencies where power reflection occurs, the maximum power transfer efficiency can only be achieved at the resonant frequencies of the system. The efficiency severely drops as the frequency of the power source deviates from the resonance frequency.
- The resonance frequency of the resonators changes as the air-gap changes.
- The copper loss and radiation loss can be greatly reduced to insignificant amounts by using resonators with high Q value.
- The frequency at which MRC can be used ranges from kHz to the GHz band.
- Obstacles between the transmitting and receiving resonators will not cause the efficiency to drop as long as the coupling and resonance can be achieved.

Based on these characteristics, there are several issues that have to be addressed for this technology to be practically used. The main ones include:

- Maintaining high efficiency by matching the resonance frequency of the resonator pair to the frequency of the power source. Maintaining this resonance is one of the core issues that has to be dealt with, and it is particularly challenging as the resonance frequency differs are different air gaps and load impedance.[16] – [19]
- Keeping the frequency of the power source within the Industrial Scientific Medical (ISM) band.
- Making an efficient power source. While this can be easily achieved in the kHz range, there are still no existing power sources for the MHz range, especially the higher power scale.
- Satisfying the safety levels for the human body.

MRC in the MHz Band

While the MRC can be conducted in a wide frequency range, ranging from kHz to GHz, this paper particularly focuses on the MHz range. Fig. 1.2 shows the sizes of a kHz and MHz resonator relative to an I-phone. Although the MHz has a disadvantage of not having efficient components and power sources, it has a big advantage of allowing smaller resonators. As a result, it will be lighter and more mobile. Furthermore, the shorter copper lines it requires will have less ohm loss, increasing the Q value of the resonator and the power transfer efficiency.

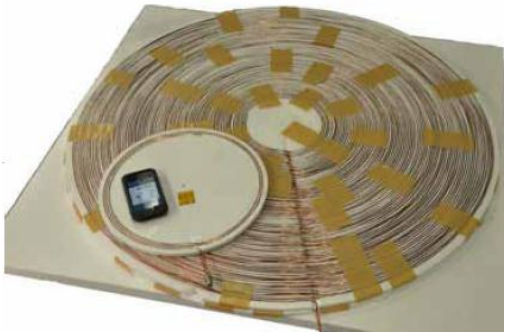

Fig 1.2. Resonators for MRC. The larger one is a 120kHz resonator, and the smaller one is a 13.56MHz resonator.

As the resonance frequency of the resonator pair changes as the impedance vary, a system to maintain resonance even at varying gap and load impedance vary is needed to maintain the high efficiency. There are many methods to conduct this such as Impedance Matching (IM) [18][19], frequency matching [20], coupling manipulation [11][21] and changing the resonator parameters [22]. Studies show that the resonance can be maintained with these matching theories. However, in the MHz range, the usable frequency range is bounded by the ISM band (13.56MHz ± 7kHz, which is very small). This means that a system to fix the resonance frequency of the resonators within the ISM band is also vital. Moreover, the matching system has to be automated to make a robust and practical system. The matching speed is also vital if we intend to transfer power to a moving target. In this case, frequency matching is not suitable as the resonance frequency often moves out of the ISM band. Manipulating the coupling in between the resonators and changing its parameters is also not practical as most systems has a fixed set of resonators that needs to adapt to different air gaps. On the other hand, IM not only satisfies the ISM boundary, it also has no moving parts in its system, which is very desirable, especially in the automotive industry.

1.2 Research Aim

This research studies the MRC WPT system which has a fixed frequency at 13.56MHz. The aim of this research is to fix the resonance frequency of the system within the ISM band, and increase its

efficiency by introducing an automated IM system. To do so, experiments and simulations were done to verify the effect of IM and viability of its automation. Then, a fast matching algorithm based on the golden section search was proposed to test the matching speed achievable and improve the robustness of the WPT system. The definition of efficiency using the voltage and current readings are also studied, and its results are compared with that of the S-parameters.

1.2.1 Main Contributions

The core topic and main contribution of this research is the automation of the IM circuit for the MRC WPT system. It can be separated into the following points

- Studying the effect of Impedance Matching on MRC [ISIE 2010][JIASC]
  - While IM is a commonly used technique to match the antennas of communication systems and to reduce the reflection in power lines, no studies has been made for MRC systems. One of the biggest differences is that the MRC resonators come as a pair because the energy is transferred to the load using an electromagnetic field. On the other hand, the antennas in communication systems sends their energy as an electromagnetic wave, thus it acts as a single antenna. The experiments and simulations conducted in this research that IM can match the frequency and increase the efficiency of the MRC system. As a result, we learnt that the maximum efficiency is not only maintained, the maximum range of WPT can also be extended using IM.
- Validating the automation of IM on MRC [EVS-25, Weva][IEEE IE journal]
  - The next step to make a robust WPT system after proving that the maximum efficiency can be achieved through IM is to prove that the IM process can be automated. This is particularly important because the WPT system has to adapt to varying air-gaps and changing loads such as a moving car or changing battery state-of-charges. Simulations done using Matlab shows that the characteristics of the transfer efficiency to the matching parameters show a single peak and a smooth gradient. This means that automation can be easily automated using even simple search algorithms. To prove this concept, the prototype IM circuit was automated using the best-step steepest gradient method to match the resonators in an experiment. The results proved the validity of automation for the IM circuit in the MRC WPT system. The experiment results also show that the efficiency achieved using the IM circuit also depends on the circuit design and components used, where a smaller and more stable circuit will achieve a higher efficiency due to less ohm loss and stray reactance.
- Improving the matching speed of the IM system using the Golden Section Search algorithm
  - The matching speed is another important factor to make a robust WPT system. This is because the efficiency should ideally be at its maximum all the time when wireless

charging to a moving object or a changing load is conducted. A fast matching algorithm will play an important role in reducing the "low-efficiency periods" of the charging process. To achieve this, a search algorithm based on the Golden Section Search technique was proposed, and experiments were conducted. The results show that the matching time is decreased to 0.15s~0.6s, which is almost 100% faster than the scaled best-step steepest gradient method used in the study above.

- Proposing a method to measure efficiency of the MHz MRC system using voltage and current.
  - In high frequencies such as the MHz range, power reflection occurs when there is mismatch, and it greatly affects the efficiency of the system. Until now, the efficiency of the IM system has been measured using the vector network analyzer (VNA), which uses the Scattering Parameters (S-Parameters). While this provides an accurate measurement of these high frequency systems, it is limited to a 50Ω system. However, in practical systems, the load impedance (such as the battery/capacitor impedance) varies as the WPT is conducted. Therefore, in this study, a method to measure the efficiency using voltage and current sensors, based on the power wave theory [][] was proposed. Simulation results of the propose method agrees with the results of the S-parameters, even at loads which are not at 50Ω. The result of the experiment which was conducted with a 50Ω load also agrees with that of the VNA.

1.3 Thesis Structure

In this thesis, the background of WPT and MRC, which serves as the research motivation, was briefly explained in Chapter 1. The research aim and the main contributions were also mentioned.

The MRC will be introduced in Chapter 2. This will include basic theories which are used to analyze the WPT system such as the equivalent circuit and frequency characteristics of MRC, as well as the definition of efficiency using the S-parameters. Additionally, the proposed method to define efficiency of such high frequency systems using voltage and current sensors will be explained.

Chapter 3 will explain the proposed automated IM system for the MRC WPT system. The necessity of the automated IM circuit will be explained, followed by the circuit diagram of the proposed IM system, and its hardware selection.

Chapter 4 is about the studies on the effect of IM on MRC. These include simulations and experiments done to confirm that the IM can increase the efficiency and power transfer range by minimizing reflection and matching the resonators. The experiments in this chapter are conducted manually using a small and compact matching circuit which consists of air core coils and ceramic condensers.

Chapter 5 is the main topic where the validity of automation for the MRC system is tested.

Simulations of the power transfer efficiency (S_{21}) versus the matching parameters were conducted to check the viability of automation. Then, experiments were conducted using the best-step steepest gradient method to prove that the automation can be executed easily with the proposed setup.

In Chapter 6, the matching speed of the system in Chapter 5 is further improved by using a matching algorithm that is based on the Golden Section Search technique. This chapter will go into detail of the algorithm flow of this proposed search algorithm. The experiment results will be analyzed and summarized. The future work that can be done to further improve on the matching time will be discussed.

Finally, the whole research will be summarized in Chapter 7, and the future topics of interest is proposed.

Chapter 2 Magnetic Resonance Coupling (MRC)

The MRC phenomenon has been explained in detail using the mode coupling theory [10] [11]. However, this theory is often complicated and inconvenient when it comes to designing the circuits around the resonators. To overcome this problem, a design and analysis method using an equivalent circuit based on antenna and circuit design theories was proposed in papers [15]-[17]. These papers show that the experimental results match the electromagnetic analysis and circuit simulations. Using the equivalent circuit, the frequency characteristics of the resonators can be estimated up to an accuracy of 5% error. [17]. In this research, the characteristics of the resonators are analyzed based on the equivalent circuits and experiments. Section 2.1 briefly explains the proposed equivalent circuit used to study MRC, and Section 2.2 explains the frequency characteristics of an MRC resonator pair.

As the aim of this research is to use MRC as a power transfer technology, the efficiency is a very important factor to consider. There are many ways to measure efficiency in a wireless power transfer system, such as the S-parameters (Vector Network Analyzers (VNA) and Directional couplers) and power electronics (Voltage and Current Sensors). Section 2.3 discusses and compares the theory and physical meaning of both methods. A method to measure efficiency using voltage and current sensors based on power wave theories is also proposed in Section 2.3.2, and comparisons of its results with that of the VNA is conducted in section 2.3.2.1.

2.1 Equivalent Circuit of MRC

WPT through MRC involves creating an LC resonance, and transferring the power through magnetic coupling without radiating electromagnetic waves.Hence the magnetic coupling can be represented as mutual inductance L_m, as in Fig 2.1. The equivalent circuit of the resonator parameters depends on the antenna design. [17] Fig 2.2 shows the prototype resonator used in this study, and TABLE I shows the shows the design of the resonators as well as the LC parameters of the antennas as measured by the VNA. As the resonator studied in this paper is an open spiral antenna, it is represented as a series set of lumped inductor *L* and capacitor *C*.

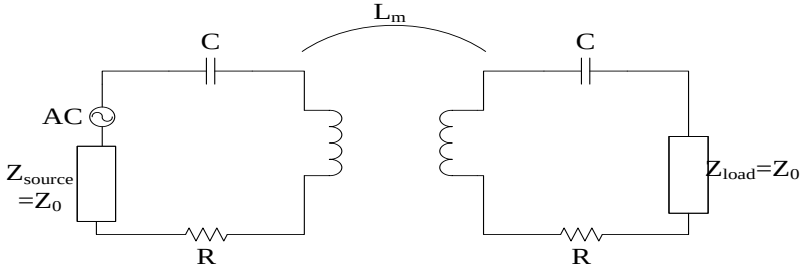

Fig 2.1. Equivalent circuit of wireless power transfer system via magnetic resonance coupling without tuning circuit.

Fig 2.2. Wireless power transfer via MRC using the prototype resonator pair used in this study.

TABLE I

PARAMETERS OF RESONATORS

Self resonance frequency	13.56MHz
Antenna type	Open, Spiral
Number of turns	5 turns
Radius	15cm
Pitch	5mm
Inductance (L)	10300nH
Capacitance (C)	13.26pF

Z_{source} in Fig. 2.1 represents the characteristic impedance of the source, and Z_{load} is the impedance of the load. In this paper, they are both set to be Z_0, 50Ω the default characteristics of most high frequency system. R represents the ohm loss and radiation loss of the resonators.

The resonance frequency of the resonator pair can be calculated based on the equivalent circuit. To satisfy the resonance condition, the reactance of Fig.2.1 must be zero, equation (2-1). This can be satisfied by two resonant frequencies as shown in equation (2-2) and (2-3). The coupling coefficient k can be derived from equation (2-2) and (2-3) into equation (2-4).

$$\frac{1}{\omega L_m} + \frac{2}{\omega(L - L_m) - \frac{1}{\omega C}} = 0 \tag{2-1}$$

$$\omega_m = \frac{\omega_0}{\sqrt{(1+k)}} = \frac{1}{\sqrt{(L+L_m)C}} \tag{2-2}$$

$$\omega_e = \frac{\omega_0}{\sqrt{(1-k)}} = \frac{1}{\sqrt{(L-L_m)C}} \tag{2-3}$$

$$k = \frac{L_m}{L} = \frac{\omega_e^2 - \omega_m^2}{\omega_e^2 + \omega_m^2} \tag{2-4}$$

Next, the efficiency of the power transfer is calculated based on the equivalent circuit. The power reflection ratio η_{11} and transmission ratio η_{21} is defined in equation (2-5) and (2-6) where S_{11} and S_{21} represent the wave reflection and transmission ratio respectively. For simplification purposes, R is considered to be 0Ω, and S_{21} can be calculated from equation (2-7) [16].

$$\eta_{11} = |S_{11}|^2 \times 100[\%] \tag{2-5}$$

$$\eta_{21} = |S_{21}|^2 \times 100[\%] \tag{2-6}$$

$$S_{21}(\omega) = \frac{2jL_m Z_0 \omega}{L_m^2\omega^2 + \left[(Z_0 + R) + j(\omega L - \frac{1}{\omega C})\right]^2} \tag{2-7}$$

2.2 Frequency Characteristics of MRC

As the gap in between the resonators change, the coupling coefficient *k* between the resonators will also vary. This causes a change in the impedance of the system, which leads to a change in resonance frequency and the power transfer efficiency.

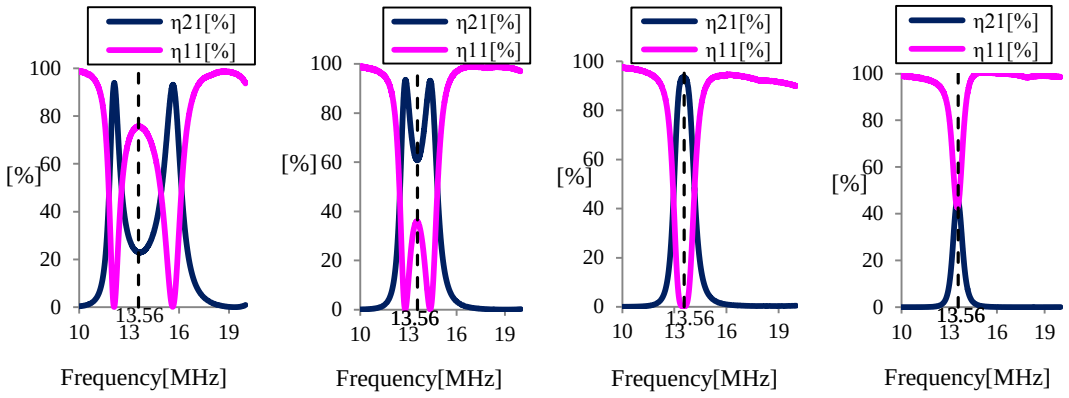

(a) gap=6cm (b) gap=12cm (c) gap=20cm (d) gap = 31cm

Fig. 2.3. Experimental results of efficiency versus frequency at different air gap.[17]

Fig. 2.3 shows the frequency characteristics of the power reflection η_{11} and transmission ratio $\eta_{21}$of the system as measured by a vector network analyzer and calculated using equation (2-5) and (2-6). The gap *g* between the resonators was varied from 6cm to 31cm. As shown in the figure, when the gaps are small and the coupling is strong, there exist two resonance frequencies that achieve maximum power transfer efficiency. As the gap becomes larger, the resonance frequencies moves closer to each other and eventually merges into one. Then, if the gap gets even larger, the maximum efficiency will drop.

2.3 Definition and Measurement of Efficiency in MRC in the MHz Range

Currently high frequency power systems (such as power sources and coaxial cables) are designed to have a common characteristic impedance, Z_0(usually 50Ω or 70Ω). The power inserted to a device, (usually through a co-axial cable) will be reflected back to the power source when the characteristic impedance of the devices in the system is not perfectly matched. This rule applies to the MRC system when it is used in the MHz range too, as the ratio of the cable length to the wavelength is large enough for the reflected power to affect the efficiency of the system.

This section discusses the various methods that can be used to measure efficiency. One is based on the S-parameter, which is commonly used to analyze travelling waves, and the other is based on the power definitions of voltage and current sensors. A method to measure the efficiency with voltage and current sensors based on power wave theories is proposed. The theory and physical meaning of

both the proposed method and S-parameter based methods are discussed in this section.

Experiment to Detect Standing Wave in the MRC WPT System at MHz Range

Before the definition of efficiency is discussed, it is important to prove that the assumption that power reflection in the MHz MRC system is true. As the reflected wave will combine with the forward wave to make a standing wave, a simple way to prove reflection occurs is to show that a standing wave is formed along the cable. To do so, a simple experiment was conducted as in Fig 2.5. In this experiment, a function generator was used to generate a 13.56MHz 5V peak-to-peak (5Vpp) wave across a 6m BNC cable to a transmitting resonator. The transmitting resonator then transfers the power to the receiving resonator that is terminated at 50Ω across an air gap through MRC. The resonators used are those in TABLE I. T-junction connectors are used at point 0m, 3m, 4.5m, 6m from the function generator to measure the voltage of the BNC cables at that point. The gaps are varied from 5cm to 25cm, and an oscilloscope was used to see the time characteristics of the voltage at those points.

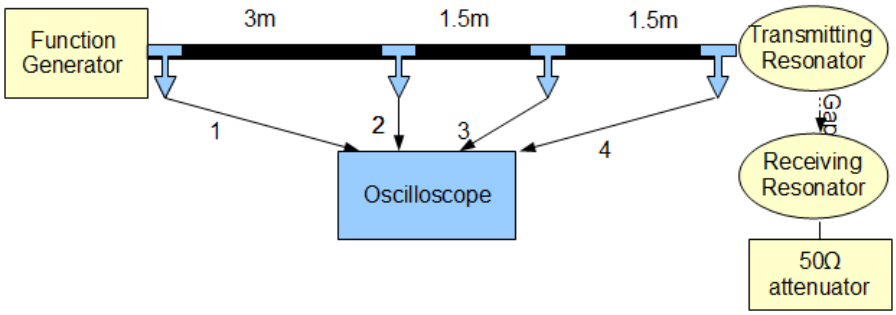

(a) Diagram of experimental setup. T-junction connectors and an oscilloscope was used to measure the voltage of the BNC at points 0m, 3m, 4.5m, 6m from the function generator.

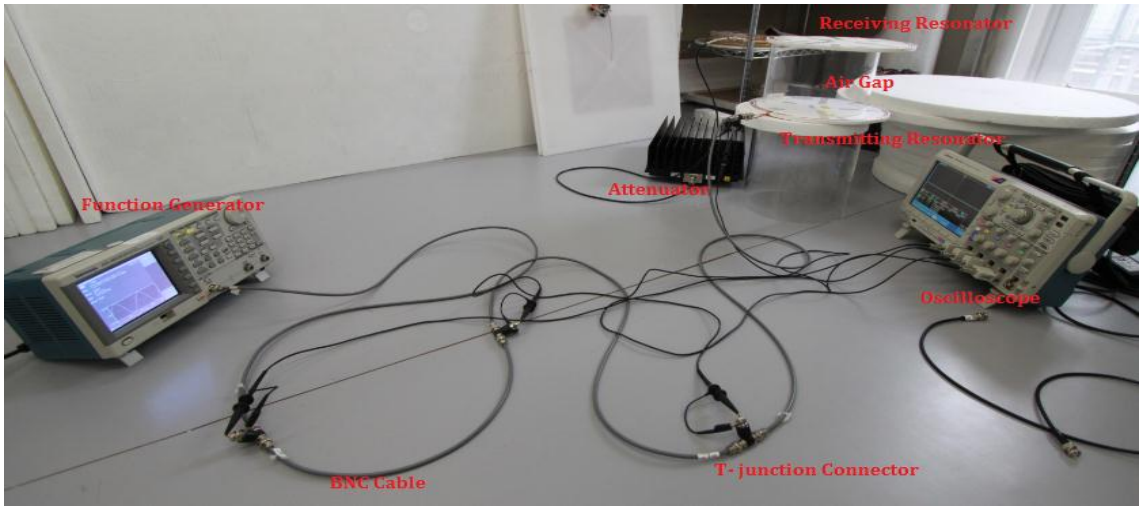

(b) Photo of experimental setup.

Fig 2.5 Experimental setup to detect standing wave in the MRC system at the MHz range

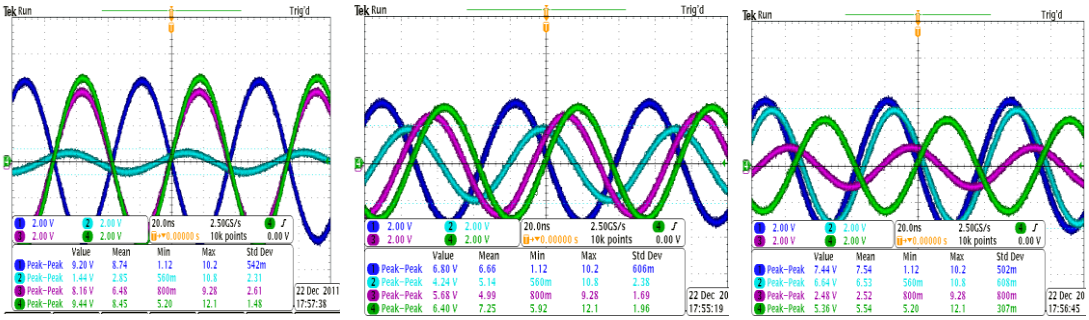

(a) Gap = 5cm (b) Gap = 15cm (c) Gap = 25cm

Fig 2.6.Experimental results. Voltagevs time at point 0m, 3m, 4.5m, and 6m from the power source. The colors for these points are in the order of blue, sky blue, magenta and green respectively. .

Fig 2.6 is the experimental results of the Voltage vs time at point 0m, 3m, 4.5m and 6m from the power source. The results clearly show that the peak voltage for each point is different, meaning the standing wave is made. The maximum peak voltage is also 10Vpp or less, showing that a reflected wave of 5Vpp or less, (depending on the reflection ratio) has stacked with the 5Vpp forward wave to form a standing wave. The difference in phase between the measurement points simply means that the resultant standing wave is propagating, a common phenomenon when it is not a full reflection. As a conclusion, the experimental results confirmed that power reflection occurs in the MHz range. It should be noted that whether or not the reflection causes a power loss depends also on the ratio of cable- length to standing wave. This means that in the kHz range, where the cables and length of the resonator coils are much shorter than the wavelength, the reflection phenomenon can be ignored and the system will obey the Ohm's law.

2.3.1 Definition of Efficiency Using S-Parameters

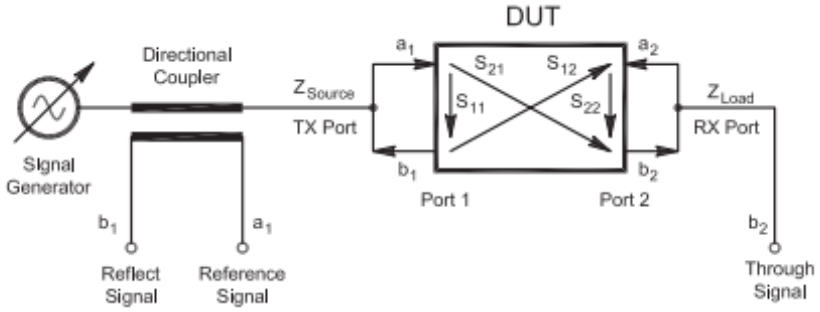

Fig 2.7. General setup to measure S-Parameters of high frequency system. [29] Here, DUT means Device Under Test

The section above confirmed that the power reflection occurs in the MRC system when it is applied in the MHz range. Fig 2.7. shows a typical setup used to measure S-parameters in high frequency systems, where a_1 represents the input power, and b_1 represents the reflected power. A

common way to define the efficiency is by S_{21} (2-7), the wave transmission ratio of the resonators. This can be easily measured by measuring a_1 and b_2 (power from the DUT to the load) using a directional coupler and calculating S_{21} with equation (2-8) and η_{21} with equation (2-6). The main advantage of using this measuring method is that it is the most accurate as both the input power and power transferred to the load is measured directly. However, it requires two directional couplers, and communication between both sides of the power transfer system, which makes the system more complicated and limited by the wireless communication speed.

$$S_{21} = \left|\frac{b_2}{a_1}\right| \tag{2-8}$$

$$S_{11} = \left|\frac{b_1}{a_1}\right| \tag{2-9}$$

$$Effiiency, \eta_{21}^{'} = (1-\eta_{11}) \times 100[\%] \tag{2-10}$$

On the other hand, S_{11} represents the wave reflection ratio of the resonators. It can be calculated using equation (2-9) using the measurements (a_1, b_1) from the directional coupler as in Fig 2.7. The power reflection ratio, η_{11} can be calculated using equation (2-5), and the efficiency of the system can be estimated using equation (2-10). Although this method is fast and simple, as only information from the power source side is required, the efficiency can only be estimated. The power loss of the resonators are not taken into consideration, making it a constant error.

2.3.2 Definition of Efficiency Using Voltage and Current Sensors

The last and most direct method of measuring the efficiency is by measuring the active input and output power. This can be done by measuring the voltage (V_1, V_2) and current (I_1, I_2) of both sides in Fig 2.1. However, as mentioned in the sections above, the power reflection occurs in high frequency systems and cannot be neglected. Moreover, as most systems do not have a fixed load impedance Z_L that matches with the characteristic impedance of the transmission line, Z_0=50Ω, the calculation for efficiency becomes even more complicated.

To do so, a method to calculate the efficiency based on the power wave theory is proposed. The power wave theory [30] is a generalized version of the travelling wave theory (S-Parameters). It is made to analyze the power travelling in and out of the system when both ends of the device are not matched to Z_0. It is a more practical analysis as most systems, including the MRC WPT system, may not have perfectly matched loads and generators, and the power input and output are generally of main concern. Naturally, the power wave theories and travelling wave theories will match when both Z_G and Z_L becomes Z_0. This flexibility serves as the main motivation for this study as most future applications of MRC will include wireless charging of batteries and capacitors, which have changing load impedances.

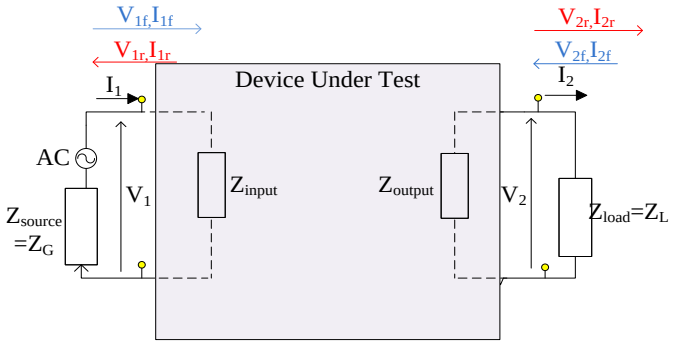

Fig 2.8. Simplification of Fig 2.1 for analysis using power waves.

To analyze the efficiency using power wave theory, the resonators in the equivalent circuit in Fig 2.1. can be simplified as Fig 2.8., where Z_{input} and Z_{output} are impedance as seen from the input and output port respectively. Here, V_{1f}, I_{1f}, V_{1r}, I_{1r}, are the voltage and current of the forward and reflected wave on the transmission line of the power source. V_{2f}, I_{2f}, V_{2r}, I_{2r}, are their respective counterparts on the load side. Based on the simplified equivalent circuit, the definition of each power waves at the power source and load side can be written as equation (2-11) and (2-12) respectively.

$$
\begin{aligned}
&Power\,Soure Side \\
&V_{1f} = Z_G^* I_{1f} \\
&V_{1r} = Z_G I_{1r} \\
&V_1 = V_{1f} + V_{1r} \\
&I_1 = I_{1f} - I_{1r} \\
&V_1 = Z_{input} I_1
\end{aligned}
\qquad \ldots (2\text{-}11)
$$

$$
\begin{aligned}
&Load\ Side \\
&V_{2f} = Z_L^* I_{2f} \\
&V_{2r} = Z_L I_{2r} \\
&V_2 = V_{2f} + V_{2r} \\
&-I_2 = I_{2f} - I_{2r} \\
&V_2 = Z_L I_2
\end{aligned}
\qquad \ldots (2\text{-}12)
$$

As the voltage V and current I are the sum of two waves in opposite directions, $V = V_f + V_r$ and $I = I_f - I_r$ are obvious. Forward waves are defined as waves that do not reflect back to the power, hence the impedance as seen by these waves are the conjugate of the impedance on the line (from the principles of conjugate matching [31]). On the other hand, as the reflected waves are waves that are reflected back and travels on the transmission line, their impedance is seen by the waves as the impedance of the transmission line. Using equations (2-11) and (2-12), the forward and reflected waves of the power source and the load side can be calculated to be equations (2-13) to (2-16).

Power Source Side :

Forward Wave

$$
\begin{aligned}
V_{1f} &= \frac{Z_G^*(V_1 + Z_G I_1)}{2\Re(Z_G)} \\
I_{1f} &= \frac{(V_1 + Z_G I_1)}{2\Re(Z_G)}
\end{aligned}
\qquad \ldots (2\text{-}13)
$$

Load Side:

Forward Wave

$$
\begin{aligned}
V_{2f} &= \frac{Z_L^*(V_2 + Z_L I_2)}{2\Re(Z_L)} = 0 \\
I_{2f} &= \frac{(V_2 + Z_L I_2)}{2\Re(Z_L)} = 0
\end{aligned}
\qquad \ldots (2\text{-}15)
$$

Reflected Wave

$$V_{1r} = \frac{Z_G\left(V_1 + Z_G^* I_1\right)}{2\Re(Z_G)}$$
$$I_{1r} = \frac{\left(V_1 + Z_G^* I_1\right)}{2\Re(Z_G)} \quad \ldots(2\text{-}14)$$

Reflected Wave

$$V_{2r} = \frac{Z_L\left(V_2 + Z_L^* I_2\right)}{2\Re(Z_L)}$$
$$I_{2r} = \frac{\left(V_2 + Z_L^* I_2\right)}{2\Re(Z_L)} \quad \ldots(2\text{-}16)$$

It is worth noticing that the forward wave from the load side is equal to zero, which agrees to the fact that no power is generated from the load. Using equations (2-11), (2-12), (2-13), (2-16), the efficiency can be calculated using equation (2-17).

$$\begin{aligned} Efficiency &= \frac{Active\ power\ into\ load}{Active\ power\ from\ source} \\ &= \frac{\Re\left(V_{2r} I_{2r}^*\right)}{\Re\left(V_{1f} I_{1f}^*\right)} \\ &= \frac{\Re(Z_L)|I_2|^2}{\left(\frac{|V_1 + Z_G I_1|^2}{4\Re(Z_G)}\right)} \\ &= \frac{\Re\left(V_2 I_2^*\right)}{\left(\frac{|V_1 + Z_G I_1|^2}{4\Re(Z_G)}\right)} \end{aligned} \quad (2\text{-}17)$$

2.3.2.1 Comparisons with S-Parameter Results

To confirm theory proposed in the section above, a simulation and an experiment was conducted to compare the results of the proposed measurement method to that of the S-parameters.

Simulation to Compare Frequency Characteristics

A simple simulation was conducted using SNAP circuit simulator to compare the results of the efficiency calculations based on S-parameters (2-6, 2-8), and the proposed method (2-17). The simulated circuit is Fig 2.9, where the parameters of equivalent circuit in Fig 2.1. is coupling factor k = 0.92, $Z_0 = Z_G$ =50Ω, Z_L = 50 + j200Ω, and R=0.77Ω.

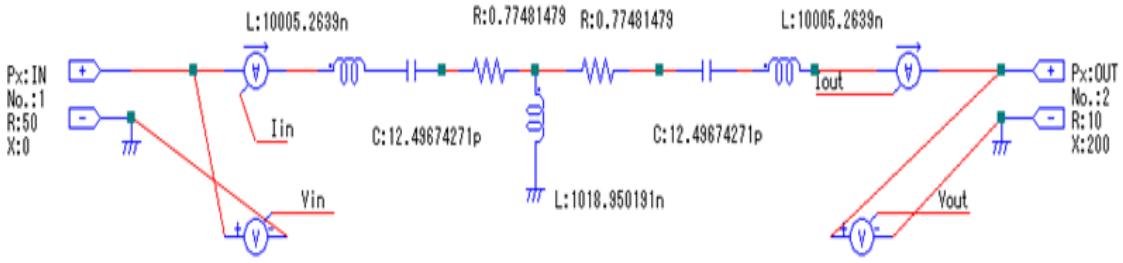

Fig 2.9 Simulation circuit with SNAP. (by Dr. Imura)

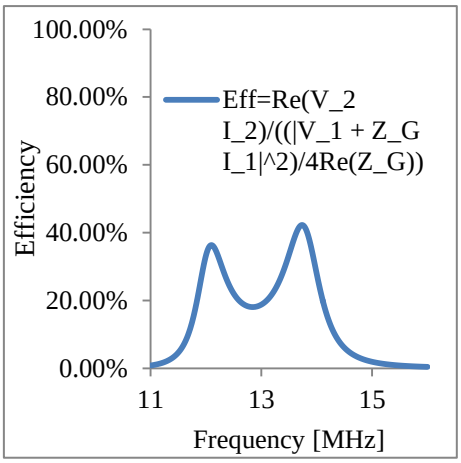

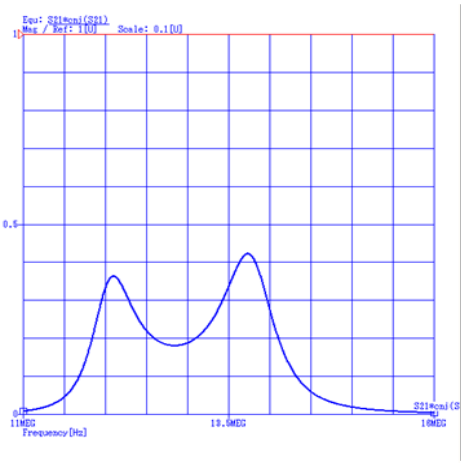

(a) Proposed method (power wave theory) (b) S-Parameters (from Dr. Imura)

Fig 2.10 Simulation results. Comparison of Efficiency vs Frequency graph of proposed method, and S-parameter.

Fig 2.10(a) shows the simulation results of the efficiency frequency characteristics defined by the proposed method which is based on the power wave theory (2-17), and Fig 2.10(b) shows the efficiency based on the S-parameters. The results above show that the frequency characteristics of both the proposed method and the S-parameters match. This means that the proposed method agrees with the S-parameters even when the impedance of the port does not match with that of the transmission line. It also shows that the measured value from both the voltage/current sensors, and the VNA agree to each other. Through these observations, it can be concluded that the simulation results show that the efficiency is defined by the ratio of active output and input power when power reflection is taken into consideration.

Experiment to Compare Efficiency vs Gap

The simulations above confirmed the proposed definition based on power wave theories. An experiment was conducted to verify the simulation results above. It is conducted using two resonators that self resonates at 13.56MHz (as in TABLE I) and set up according to Fig 2.11. The efficiency is measured in two ways. The first method uses a VNA to measure the power transmission ratio η_{21}., and the second method uses a function generator to generate 13.56MHz, and an oscilloscope to measure the voltage and current of each side of the antennas in Fig 2.1. The gaps were varied from 5cm to 24cm, and the efficiency of both methods was compared. Due to the constraints of the VNA, the experiment was conducted with the conditions of $Z_0 = Z_L = Z_G = 50\Omega$.

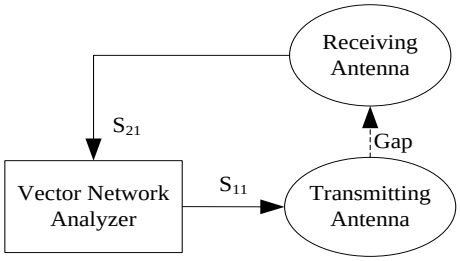

Fig 2.11. Experimental setup to measure wave transmission ratio η_{21} with VNA. (S-Parameters)

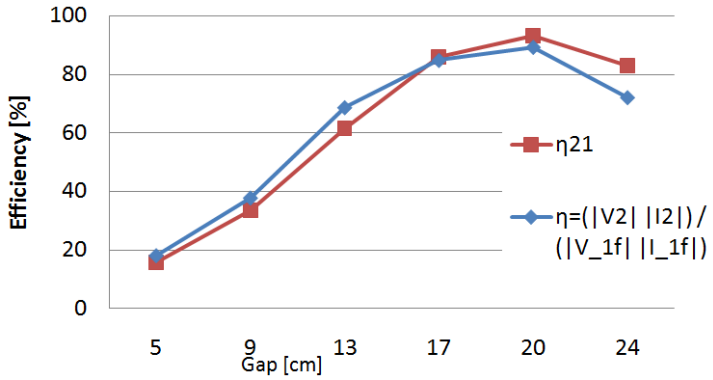

Fig 2.12. Experimental results. Efficiency vs Gap. The red line is the measurement results of the VNA (S-parameters), and the blue line is the calculated results based on the voltage and current measurements (proposed definition based on power waves)

The results in Fig 2.12 verify that both efficiency measurement methods agree with each other. Therefore, it shows that to correctly define and measure efficiency in high frequency systems such as the MHz band MRC, the power reflection has to be taken into consideration. Like regular power electric definitions of efficiency, the active power is the measured value.

Chapter 3 Proposed Automated Impedance Matching System

Chapter 2 gave a brief explanation on the basic theory and the characteristics of MRC, and discussed how the power reflection that is caused by the mismatch of impedances will lead to a loss in efficiency. This chapter explains in detail the proposed automated Impedance Matching (IM) system. Section 3.1 discusses the importance of an automated IM system to maintain the efficiency of the MRC, and section 3.2 explains in detail the setup of the proposed system. Lastly, as previous studies showed that the components used in the matching circuit will greatly affect the efficiency and the matching speed of the system, the hardware of the setup is discussed in section 3.3.

3.1 Necessity of Automated IM System for MRC

The frequency characteristic in Fig. 2.3 shows that the resonance frequency of the MRC system changes as the gap changes. There is a need to match the resonance frequency of the resonators to the frequency of the power source to create a highly efficient WPT system that is robust to positional displacements. Moreover, when applied in the MHz band, the usable frequency for the WPT is limited by the Industrial Scientific Medical (ISM) band (Fig 3.1). For example, the frequency range that is used in this research is the 13.56MHz band, which is limited to 13.56MHz±7kHz. This frequency range is much narrower compared to the change in frequency caused by a varying air gap. Finally, the speed of the matching process also has to be fast in order to constantly maintain resonance as the air gap between the resonator pair change. In other words, the conditions for the matching system in the MHz MRC system are that it has to have: a fixed power source frequency, fixed resonance frequency, and fast matching speed.

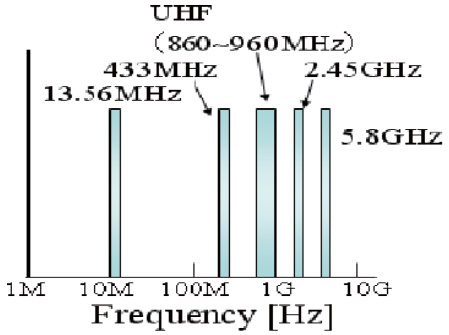

Fig 3.1 Industrial Scientific Medical (ISM) band.The frequency range which can be used for purposes other than communication.

As mentioned in Chapter 1, there are many methods to match the frequency of the resonator pair to the frequency of the power source, from the proposed Impedance Matching [18][19], to other choices such as frequency matching [20], coupling manipulation [11][21], and changing the resonator parameters [22]. However, the frequency matching method is limited by the ISM band,

which is too narrow in the MHz range. This causes the system to be limited in usable air-gaps, defeating one of the main advantages of this mid-range WPT technology. Coupling manipulation involves changing the air gap in between the resonators so that the resonance frequency matches the power source frequency. This is also not practical as most practical systems will require the WPT system to adapt to the varying air gaps, not the other way round. Lastly, the parameters of the resonators also cannot be easily changed as it is fixed by the size and design of the resonators.

Therefore, it is clear that of the methods mentioned above, only the IM method satisfies the first two conditions mentioned. The matching speed can also be increased by using an appropriate search algorithm to find the matching parameters.

Basic Theory of Impedance Matching

The IM is a technique commonly used in the power transfer and communication industry to improve the efficiency of the system. It is usually done by inserting a matching network such as in LC circuit to minimize the wave reflection ratio. Fig 3.2 represents a simple circuit with an AC source. The characteristic impedance of the source is defined as Z_{source} and the load impedance is defined as Z_{load}. The power transferred to the load can be written as in equation (3-1), and it reaches its maximum when $Z_{source} = Z^*_{load}$ to make equation (3-2). In other words, the circuit is matched and its efficiency maximized when the impedance of the load from the source's point of view matches the conjugate of Z_{source}, vice versa.

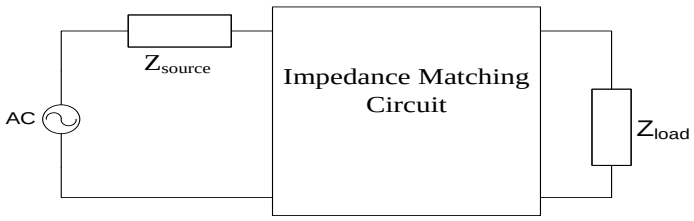

Fig 3.2 Equivalent circuit explaining the common structure of an IM system

$$P_{load} = I^2 Z_{load} = \frac{V^2}{Z_{source}} \left(\frac{1}{\frac{Z_{source}}{Z_{load}} + 2 + \frac{Z_{load}}{Z_{source}}} \right) \tag{3-1}$$

$$P_{\max} = \frac{V^2}{4Z_{source}} \tag{3-2}$$

$$\begin{pmatrix} V_1 \\ I_1 \end{pmatrix} = \begin{pmatrix} A & B \\ C & D \end{pmatrix} \begin{pmatrix} V_2 \\ I_2 \end{pmatrix} \tag{3-3}$$

$$Z_{source} = \sqrt{\frac{AB}{CD}} \tag{3-4}$$

$$Z_{load} = \sqrt{\frac{DB}{CA}} \tag{3-5}$$

The IM circuit can be considered a two-port network that is described in equation (3-3). The matching conditions are satisfied when the parameters satisfy equations (3-4) and (3-5). There are three main types of impedance matching circuits, namely the L-type, π-type and the T-type IM circuit topographies. The L-type has the simplest design of the three, but it has a lower performance as it has the lowest system Q-value. The π-type and the T-type matching circuit allows us to control the Q value of the system, thus reaching a better performance. However, their designs are more complicated, and the Q value of its components also has to be equally high, meaning they are required to have a low ohm loss. In this research, the L-type matching circuit is used to match the resonance frequency of the resonators to the frequency of the power source.

3.2 Setup of Proposed Automated IM System

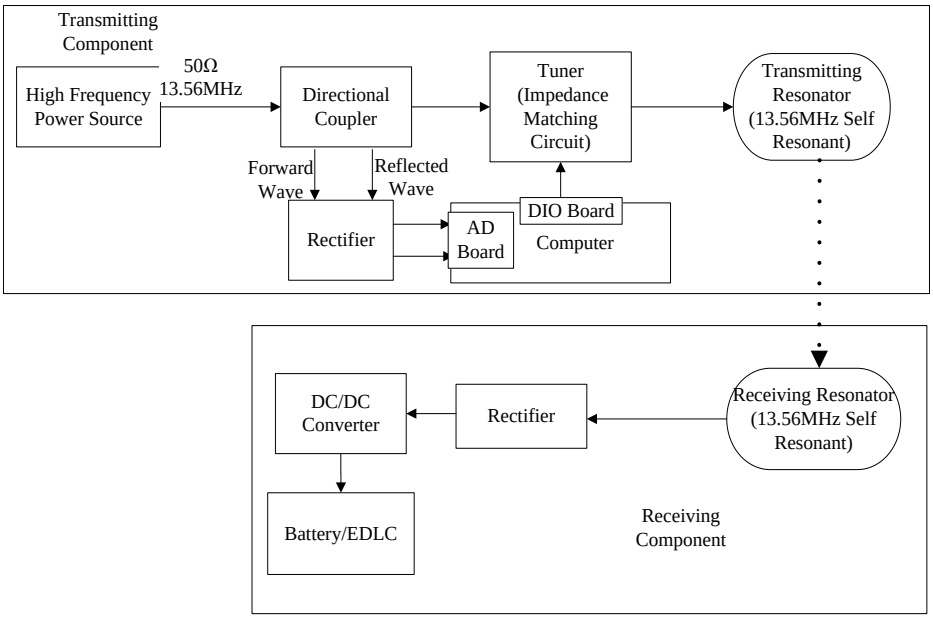

Fig 3.3 Proposed MRC WPT with automated IM system

Based on the theory explained above, an automated IM system is designed to match the resonators in the MRC based WPT system. Fig 3.3shows a diagram of the proposed automated IM in the MRC WPT system, and Fig 3.4 shows its equivalent circuits when both types of L-type matching circuits (L-type and Inverted L-type) are inserted into the system. It is modified from Fig 2.1 by inserting a two port IM circuit before the transmitting resonator, and converting it into a T-type equivalent circuit. The system transfers the power from the 13.56MHz power source to the load through the two resonators with identical self-resonance frequency. The power is transferred through MRC between the resonators, and it is rectified to charge energy storage mediums such as batteries and capacitors.

The characteristic impedance of the power source and the BNC cables are 50Ω in this paper, the typical characteristic impedance of high frequency systems. Under normal circumstances, the coupling coefficient *k* (affected by the air gap) between the resonators, and the impedance of the load (set to 50Ω in this paper) are unknown and variable. Only the voltage, current, and wave reflection ratio can be measured in the transmitting side of the system.

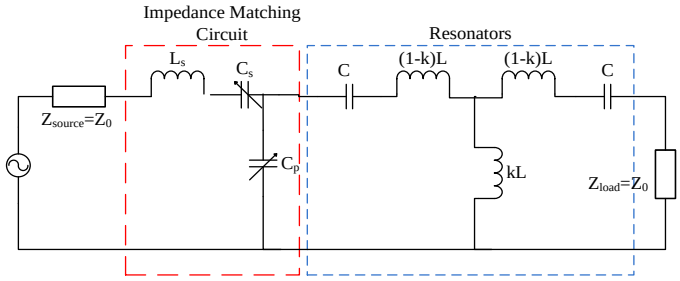

(a) L-type matching circuit

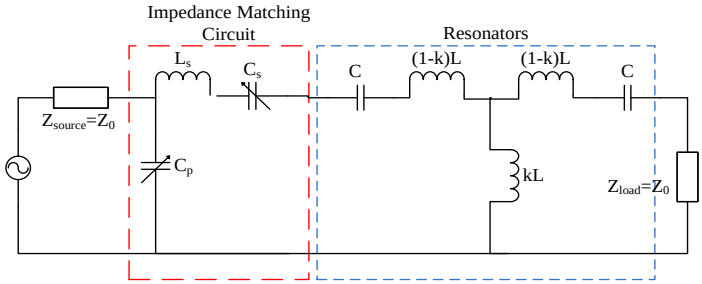

(b) Inverted L-type matching circuit

Fig 3.4.Equivalent circuit of the proposed system.

In the proposed system, a directional coupler (Fig 3.5) is inserted between the power source and the transmitting resonator to measure S_{11}, the ratio of power that is reflected from the resonators back to the power source. The directional coupler does it by coupling 40dB of the forward wave and reflected wave from the main transmission line to the measurement line. The measured values are rectified (Fig 3.7) and input into a computer which is used to control the parameters of the IM circuit. The rectifier is a simple analog circuit made up of two amplifiers and a diode. The first amplifier amplifies the AC signal from the directional coupler so that the error through the non-linearity and cut-off voltage of the diode can be minimized. Then, after rectifying and smoothed, the signal is amplified again so that it optimizes the signal-noise ratio and precision of the AD board. In this case, the reflected wave is amplified more than the forward wave so that the precision and accuracy of its readings at low reflection ratios can be increased.

While the final target of the system is to charge batteries and capacitors, in the experiments in this paper, the load is fixed at 50Ω with an attenuator (Fig 3.6) for simplification purposes. This also allows the efficiency to be measured using the VNA, which increases the reliability of the efficiency

analysis.

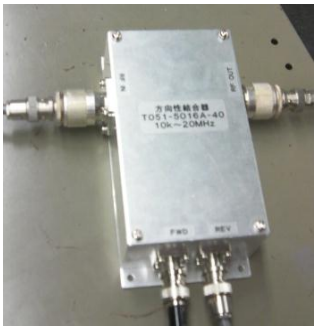

Fig 3.5. Directional coupler used to measure the forward and reflected wave in the cable.

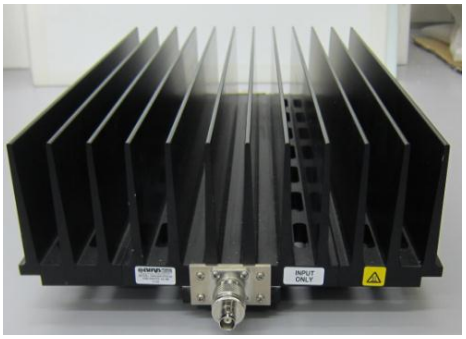

Fig 3.6. Attenuator used as 50Ω load in the automation experiments.

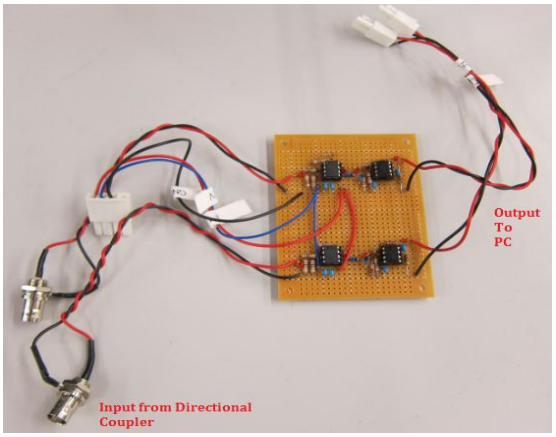

(a) Photo of the rectifying circuit with its amplifiers

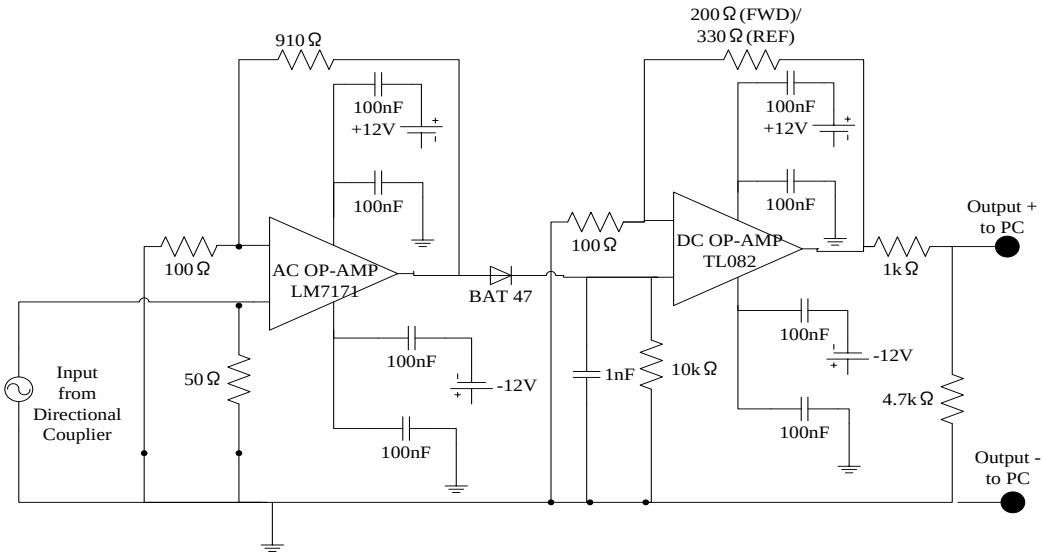

(b) Equivalent circuits of the rectifying circuit between directional coupler and PC

Fig 3.7. Rectifying circuit with amplifiers used to input the readings from the directional coupler to the PC. In this system, the reflected wave (REF) is amplified more than the forward wave (FWD) to minimize the error of the signal readings. This difference is compensated (with software) in the

calculation process for S_{11}. The amplifications were chosen so that the error through the non-linearity and cut-off voltage of the diode, and signal-noise-ratio can be minimized, while staying safe within the 10V limit of the AD board.

The main advantages of using this system are:

- Simplicity –This system only requires information from the transmitting end of the system, meaning communication systems in between the two ends of the power transfer system is not required. As a result, the complication of transmitting weak communication signals over the strong magnetic field can be avoided, making it cheap and simple. Moreover, the proposed system only uses the reflected wave ratio from the directional coupler. While its performance may not be as good as other complicated systems that use parameter estimations, its simplicity allows it to be more robust against parameter errors which occur during the production of the resonators.
- Does not require space at the receiver end –Another advantage that must be taken seriously is that the proposed system uses the space only in the transmitting end for the IM circuit. In practical applications such as EV or mobile appliance charging, this plays an important roleas the receiver (mobile appliances) should not be burdened with extra space and weight, which lowers is mobility. On the other hand, the transmitting end (charger) is usually stationary, and can afford to have more space and weight, as mobility is not an issue.
- No moving parts – As the IM circuit is controlled using electrical components, it does not involve moving parts. As a result, it simplifies the mechanical design of the systems, and requires less maintenance. This is particularly important in the automobile industry as it severely complicates the design of the vehicles.

3.3 Hardware Selection of Proposed IM Circuit

As the IM circuit is an LC circuit (Fig 3.4), there are many ways to make this circuit. These include the choice for the inductors (air-core coil, ferrite core coil), and capacitors (Variable capacitors, ceramic condensers, vacuum capacitors). Previous studies show that the Q-values of the components used in the IM circuit affect the efficiency of the system. [28] [32]As this research requires an efficient circuit as well as a fast matching speed, a prototype matching circuit has been created using air-core coils, ceramic condensers and high frequency relays on a Print-Circuit-Board (PCB) using the EAGLE software and the PCB milling machine (Fig 3.9). Fig 3.8(a) shows the photo of the prototype IM circuit, and Fig 3.8(b) is its equivalent circuit. In this prototype, multiple ceramic condensers connected in parallel, and two air core coils (L_1 = 4μH and L_2 = 1.4μH) were used in combination with high frequency relays that act as switches. The relays act as switches to select the matching parameters, and are controlled using the computer through the Digital Input-Output (DIO) board. As in Fig 3.8(b), the layout was set such that both the L-type and inverted

L-type matching circuit can be realized. The IM circuit can also be bypassed (Thru) to test the reflected wave ratio of the antennas without the IM circuit, and to minimize the ohm loss (due to components) if IM is not necessary.

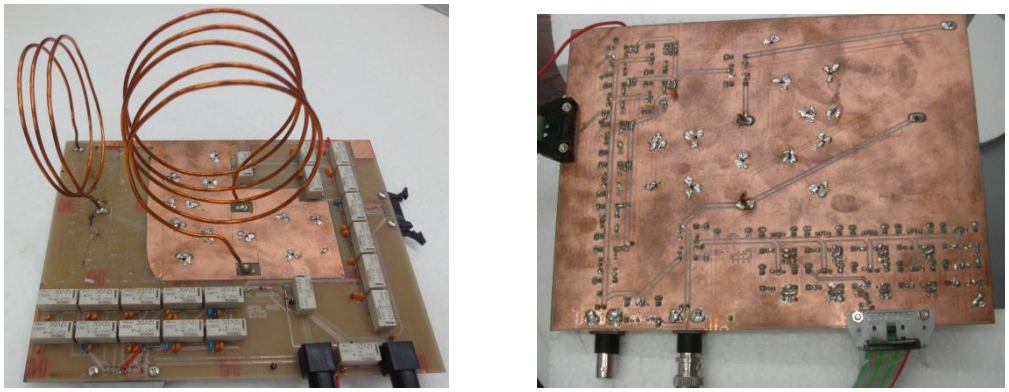

(i) Top view (ii) Bottom View

(a) Prototype IM circuit

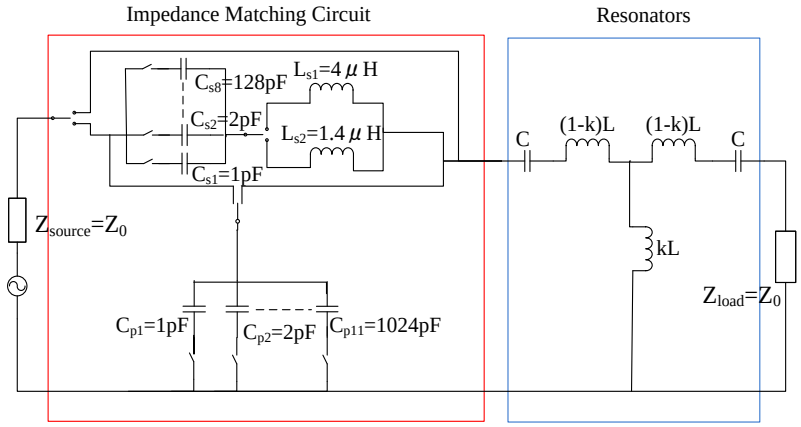

(b) Equivalent circuit of prototype

Fig 3.8. Prototype IM circuit used in the automation experiments. (Chapter 5 and 6) and its equivalent circuit. The equivalent circuit is the extension of the equivalent circuit in Fig 3.3, where multiple high frequency relays act as switches to choose the required matching topography and parameters (air-core coils and ceramic condensers).

This hardware setup satisfies the first requirement (high Q-value) because both the components used, (ceramic condensers and air core coils) are very stable and have very low ohm loss even at high frequencies. Moreover, the PCB board used allows the AC compartment to travel across a wider surface area, thus lowering the ohm loss (due to skin effect). The PCB is also designed to be compact, minimized AC lines surfaces facing each other, and with stable grounding to get rid of possible stray reactance. On the other hand, the choice of using high frequency relays to select the parameters allows the system to have a faster matching speed. This is because the physical limit of the matching speed is only determined by the chattering of the reed relays (5ms in this paper), as

high frequency systems have an extremely fast response. This is significantly faster than the more commonly used variable condensers that are controlled by motors, which have a sampling rate of several ms. For high power situations, the ceramic condensers can be replaced with high Q components such as vacuum capacitors. In the following automation experiments, the sampling time is 1ms, and the S_{11} is calculated from the average of five samples.

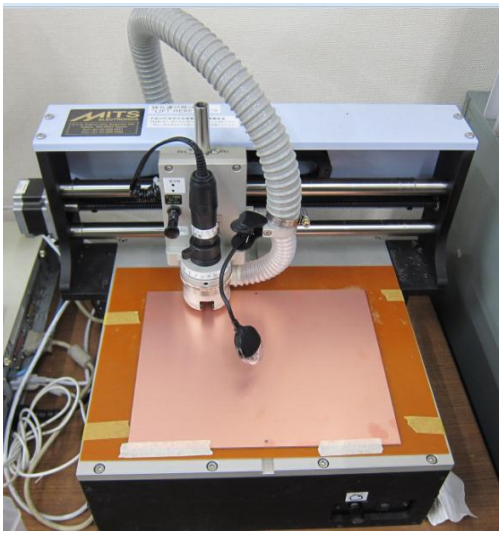

Fig 3.9 PCB milling machine used to make the prototype IM circuit.

Chapter 4 Study on the Effect of Impedance Matching on MRC

Before the experiments for automation can be conducted, it is vital to study the effect of IM on the MRC. This chapter focuses on confirming that the IM can increase the systems efficiency through matching the resonators, and to see how much an IM circuit can increase the efficiency, and range of the MRC WPT system. First, a simulation was conducted using the LT-Spice circuit simulator to verify the IM theory, and an IM experiment was conducted manually to see the maximum efficiency and range achievable through IM.

4.1 Simulation to Study the Effect of IM on MRC

The simulation to study the effect of IM was done using LT-Spice, which calculates the efficiency based on S-parameters. The equivalent used in the simulation is in Fig 4.1 (similar to Fig 3.4). Two types of L matching circuit topography were tested, namely the L-type (Fig 4.1(a)) and the inverted L-type matching circuit (Fig 4.1(b)). According to IM theories, the L-type matching topography is used when the impedance of the load (right) end of the matching circuit is higher than that of the source (left) side. This occurs when the coupling is strong, (k > 0.06 in for the resonator pair used in this research, small air gap) and two resonance frequency exists. Likewise, inversed L-type matching topography is used when the impedance of the load is lower than that of the source, which happens when the coupling is weak and only one efficiency peak exists (large air gap). In this simulation, both conditions were tested, one where the k = 0.17 (strong coupling, small air gap), and the L-type matching circuit is used, and one where k = 0.03 (weak coupling, large air gap), and the inversed L-type matching circuit is used. For simplification purposes, the ohm loss of the antennas R, are considered to be zero in this simulation.

The simulation results in Fig 4.2 show that the frequency characteristic of the power transmission η_{21} and reflection ratio η_{11}. The efficiency of the system is defined as η_{21}, and it reaches maximum when resonance occurs (η_{11} becomes zero). The results verify that the L-type IM circuit (Fig. 4.2(a)) can be used when the frequency splitting occurs to shift the resonance frequency to the frequency of the power source, thus increasing the efficiency. On the other hand, the inverted L-type matching circuit (Fig 4.2(b)) improves the efficiency by creating a sharper peak at the resonance frequency.

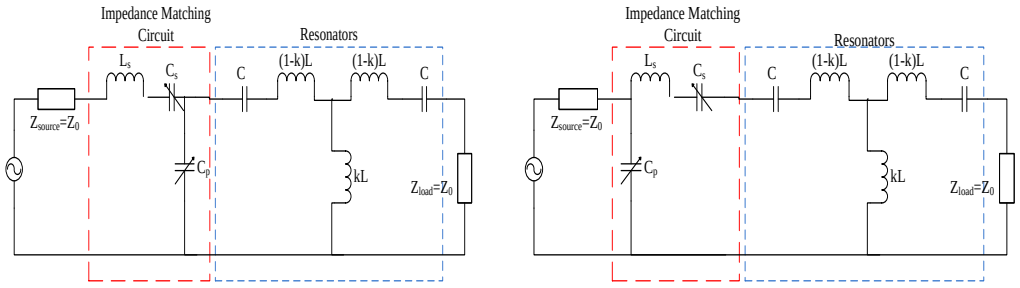

(a) L-type matching circuit (b) Inversed L-type matching circuit

Fig 4.1. Equivalent circuit of simulation and experimental setup to confirm effect of IM circuit

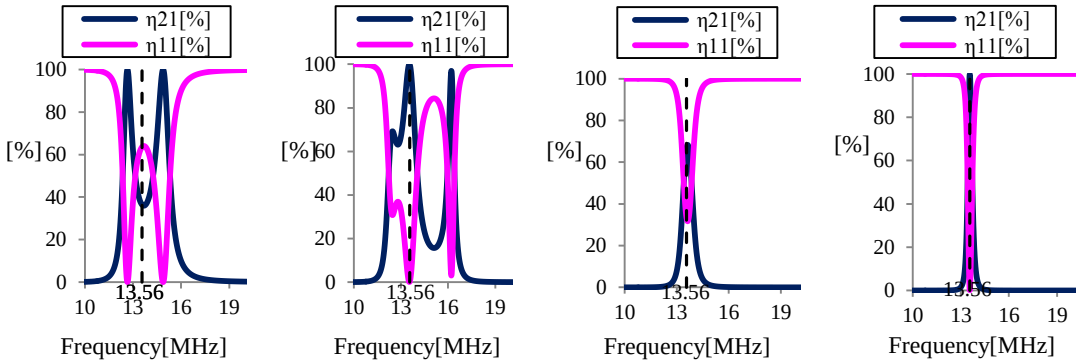

(i) Before matching (ii) After matching (i) Before matching (ii)After matching

(a) L matching circuit (k = 0.17) (b) Inversed L matching circuit (k = 0.03)

Fig 4.2. Simulation results. Frequency characteristics of the system before and after matching

4.2 Manual Matching Experiment to Study the Effect of IM on MRC

The simulations above show that the IM can potentially increase the efficiency and power transfer range of the MRC system, by shifting the resonance frequency or by making a sharper peak at the resonance frequency. Although it shows that the efficiency can theoretically be maximized to 100%, other factors such as the ohm loss (which affects energy loss) and total impedance (affects transferable power and energy loss) of the system must also be taken into consideration. For example, when the coupling is weak (large gap, single peak), the overall impedance of the system will be low. As a result, even a slight ohm loss in the antennas will lead to a big loss in the system, thus limiting the range at which the MRC WPT can be conducted even with IM. The experiments here are conducted to see the potential of IM in practical systems.

4.2.1 Experimental Setup

This experiment is conducted using the 13.56MHz resonator pair with the TABLE I parameters. Fig 4.3(a)(i) shows the resonator pair used in the experiment. The setup was as in Fig 4.3(b), where an IM circuit is inserted between the power source (VNA) and the transmitting resonator (bottom in Fig 4.3.(a)(i)). The equivalent circuit of this experimental setup is as in Fig 4.1, similar to the simulation. The IM circuit (Fig 4.3. (a)(ii)) was made using air-core coils and ceramic condensers so that the loss can be kept to a minimum. The IM circuit is also kept as compact as possible so that the effect of stray reactance can be limited. Hence, the results obtained by this IM circuit can be considered the close to the maximum potential of the IM.

In this experiment, the resonator pair is coaxial, and the gap is varied from 6cm to 43cm. The VNA was used to measure that the wave transmission ratio S_{21} and wave reflection ratio S_{11}. The power transmission ratio η_{21} (efficiency) can be calculated using equation (2-6). The L-type matching circuit is used for gaps up to 20cm, and the inverted L-type matching circuit is used for gaps bigger than 20cm.

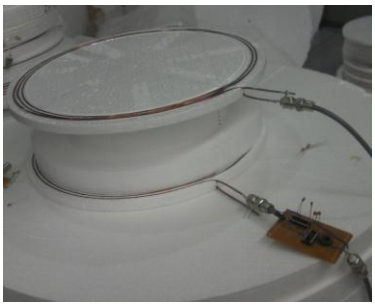

(i) Resonator pair with IM circuit connected to transmitting resonator

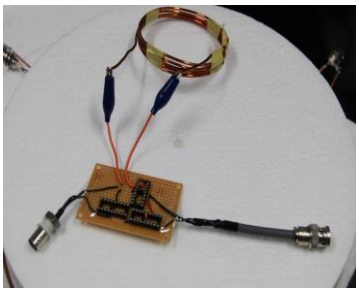

(ii) IM circuit made of air core coil and ceramic condenser

(a) Photo of resonator pair and IM circuit used in manual matching experiment.

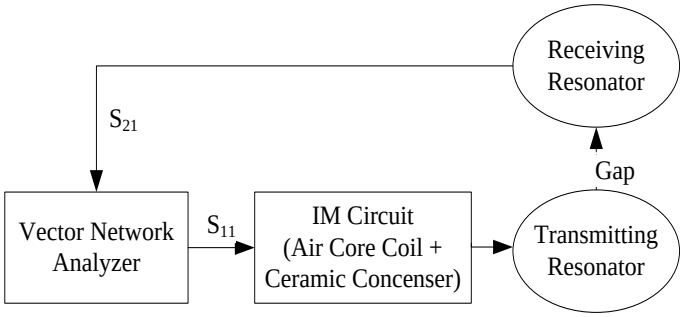

(b) Diagram of experimental setup.

Fig 4.3. Experimental setup for manual matching. The VNA is used to measure the wave transmission and reflection ratio. The gap between the resonators are varied from 6cm to 43cm.

4.2.2 Experimental Results

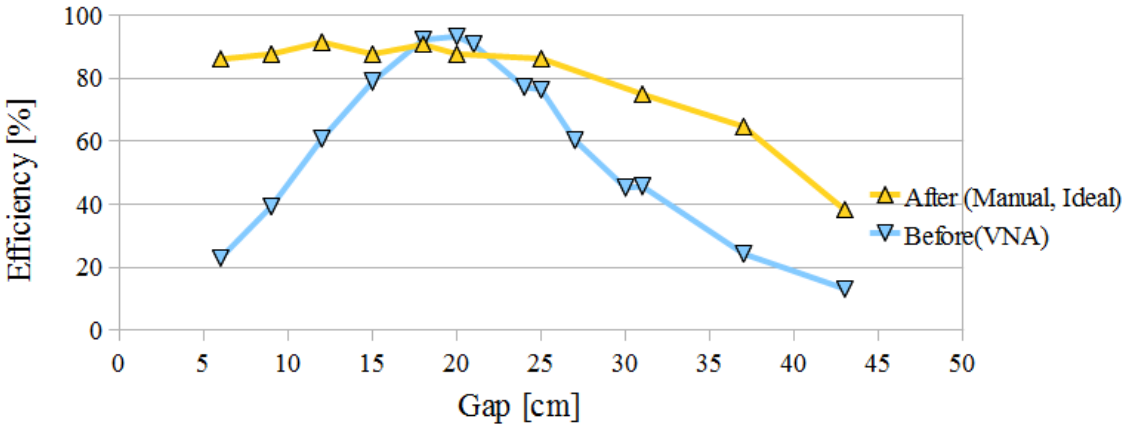

Fig 4.4 Experimental Results. Efficiency vs Gap before and after matching.

Fig 4.4 shows the efficiency of the MRC system before and after IM is conducted using the IM circuit mentioned above, and Fig 4.5 and Fig 4.6 shows the frequency characteristics of η_{21} and η_{11} for each gap before and after matching respectively. The results in Fig 4.4 show that the IM circuit

can increase the efficiency of the MRC system to 85%, almost equal to the maximum potential of the efficiency of the resonator pairs. This is particularly true when the coupling is strong, and frequency splitting occurs. The L-type matching circuit here will shift the resonance frequency to 13.56MHz, thus increasing the efficiency. (Fig 4.5(a)-(e) and Fig 4.6(a)-(e)) Of the 15% of efficiency loss, approximately 5% is due to the ohm loss and radiation loss of the resonators, as the maximum efficiency potential of the resonators is also 95% (Fig 4.5). The other 10% is mainly due to the ohm loss of the components used in the IM circuit.

At gaps larger than 20cm, the coupling becomes weak and only one peak exists. As with the simulation results above, the inversed L-type matching circuit used here can increase the efficiency by making the peak at the resonance frequency sharper (Fig 4.5(g)-(j) and Fig 4.6(g)-(j)). However, as this matching circuit lowers the overall impedance of the system, it becomes more sensitive to the other ohm loss, thus causing the maximum efficiency to drop. Therefore, the larger the air gap, the lower the efficiency achievable through IM. For this particular pair of resonators, the IM can increase the power transfer range to approximately 34cm while keeping the efficiency above 70%.

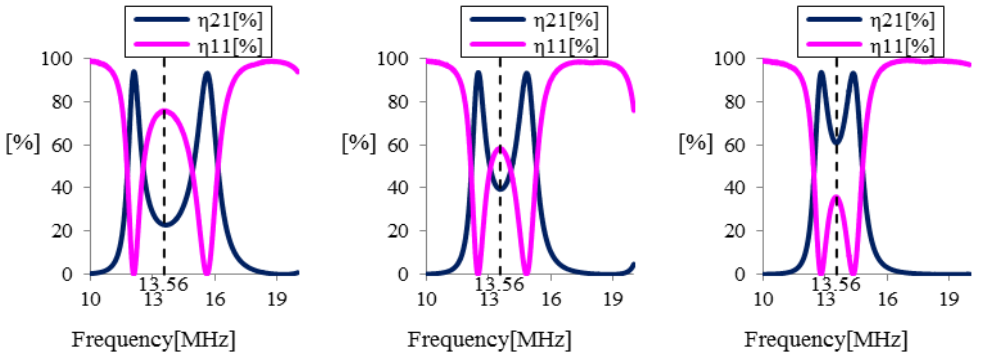

(a) Gap = 6cm (b) Gap = 9cm (c) Gap = 12cm

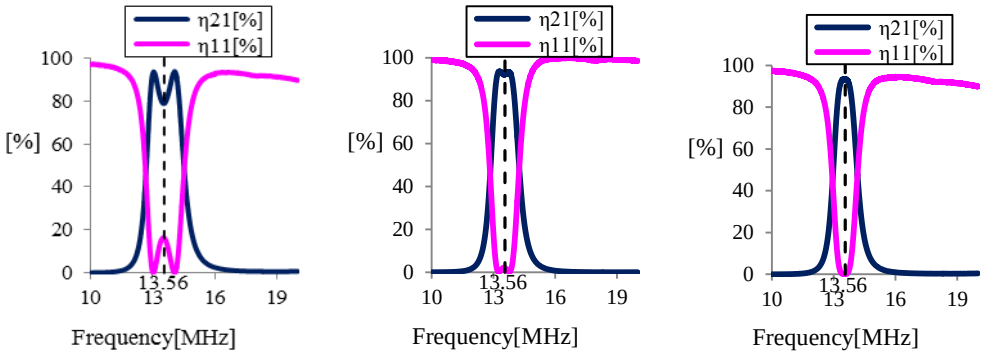

(d) Gap = 15cm (e) Gap = 18cm (f) Gap = 20cm

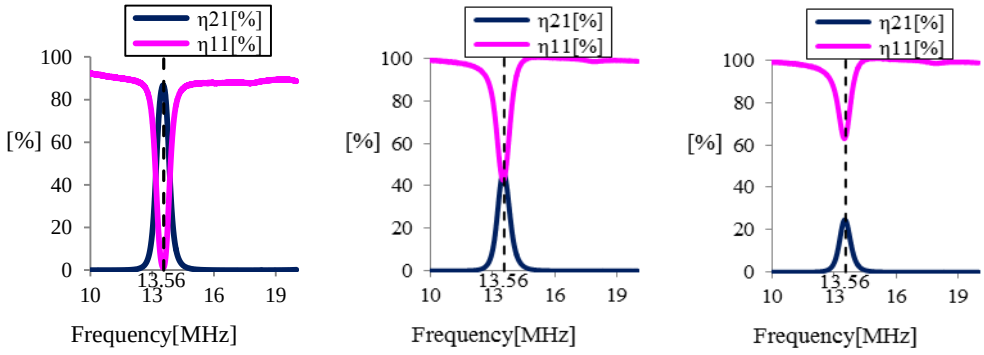

(g) Gap = 25cm (h) Gap = 31cm (i) Gap = 37cm

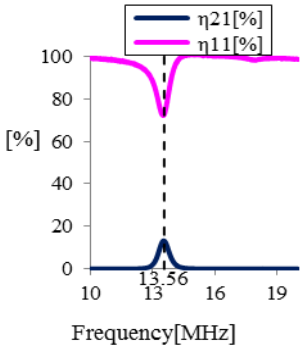

(j) Gap = 43cm

Fig 4.5 Experimental results. Frequency characteristics of resonator pair before IM for gap=6cm to 43cm

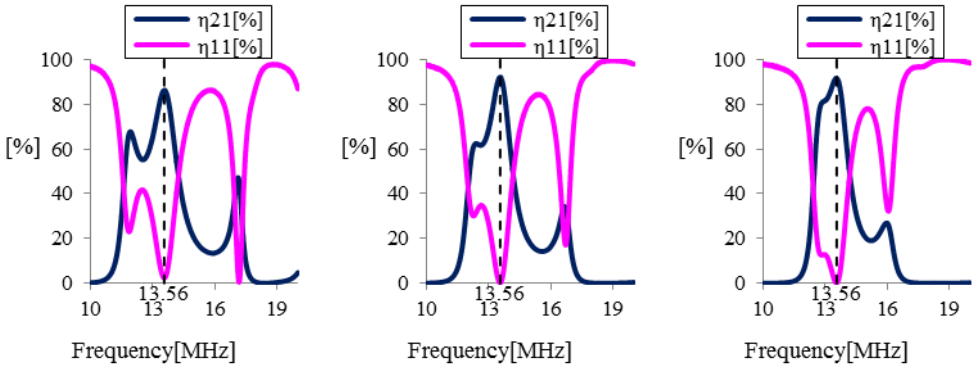

(a) Gap = 6cm
L-type, L_s = 3.88μH,
C_s = 56pF, C_p = 31pF

(b) Gap = 9cm
L-type, L_s = 3.88μH
C_s = 51pF, C_p = 35pF

(c) Gap = 12cm
L-type, L_s = 3.88μH,
C_s = 42pF, C_p = 51pF

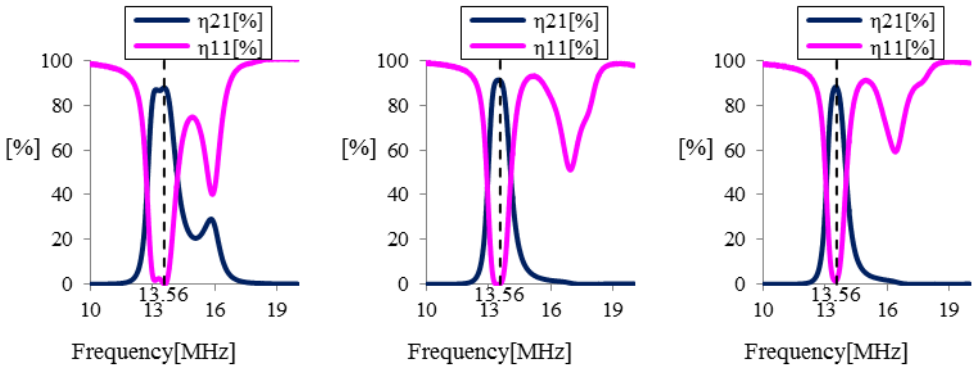

(d) Gap = 15cm
L-type, L_s = 3.88μH,
C_s = 37pF, C_p = 59pF

(e) Gap = 18cm
L-type, L_s = 3.88μH
C_s = 33pF, C_p = 34pF

(f) Gap = 20cm
L-type, L_s = 3.88μH,
C_s = 32pF, C_p = 48pF

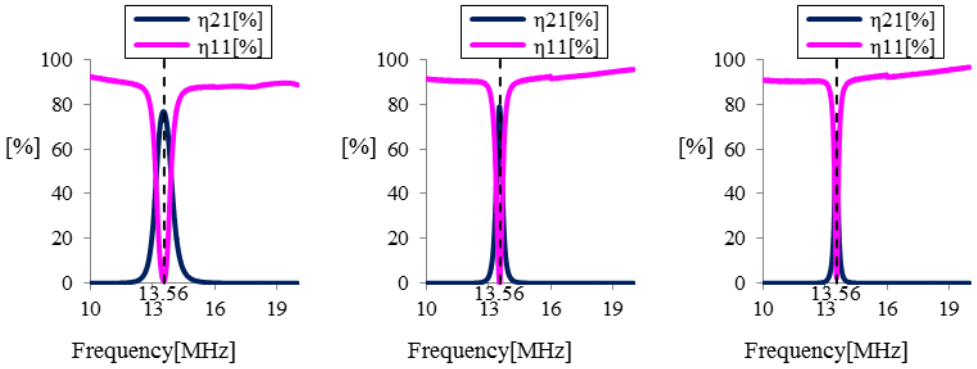

(g) Gap = 25cm
Inverted L-type, L_s = 1.43μH,
C_s = 110pF, C_p = 220pF

(h) Gap = 31cm
Inverted L-type, L_s = 1.43μH
C_s = 102pF, C_p = 440pF

(i) Gap = 37cm
Inverted L-type, L_s = 1.43μH,
C_s = 98pF, C_p = 540pF

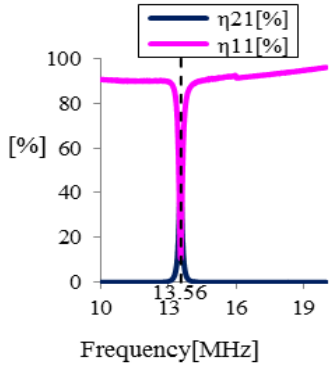

(j) Gap = 43cm

Fig 4.6 Experimental results. Frequency characteristics of resonator pair after IM for gap = 6cm to 43cm.

4.3 Summary

As a conclusion, a compact and low loss IM circuit has been created to manually match the resonators. The simulation and experimental results show that IM can increase the efficiency by matching the resonance frequency of the resonators to the power source, and by creating a sharper peak at the resonance frequency. Resonation can be induced at a fixed frequency even when the coupling coefficient (air gap) is varying. The maximum efficiency that can be achieved with this low loss IM circuit is 85%, and the range where the efficiency is above 70% can be increased to 30cm. If IM is automated, it can potentially maintain the maximum efficiency for gaps up to 30cm, increasing the flexibility and robustness of the system.

Chapter 5 Automation Validation of IM on MRC

This chapter focuses on proving that the proposed system in Fig 3.3 can be automated to make it robust towards positional displacements. To do so, the S_{21} characteristics when then matching parameters (C_s, C_p) changes is studied through a simulation using MATLAB. Then, the prototype IM circuit in Fig 3.8 was tested using an experiment setup based on Fig 3.3. The matching algorithm used to test its viability is explained in section 5.2.1. Finally, the results of the experiments using the Best-Step Steepest Gradient (BSSG) method based search algorithm are discussed in section 5.2.2.

5.1 Simulation of S_{21} Characteristics versus Matching Parameters

The previous chapter verified that the efficiency of the resonators can be improved using an IM circuit. To assist in the automation design, it is vital to know how the transmission and reflection ratio change as the matching parameters change so that a suitable matching algorithm and hardware design can be chosen. For example, if local peaks exist, a more sophisticated matching algorithm such as the particle swarm optimization will need to be implemented instead of simple two dimensional optimization algorithms such as the steepest gradient method. The sharpness of the peak will also determine the precision of the tuning parameters and matching algorithm required. Therefore, a simulation was conducted using MATLAB to study the characteristics of S_{21} as the capacitance of the matching parameters (C_s, C_p) change.

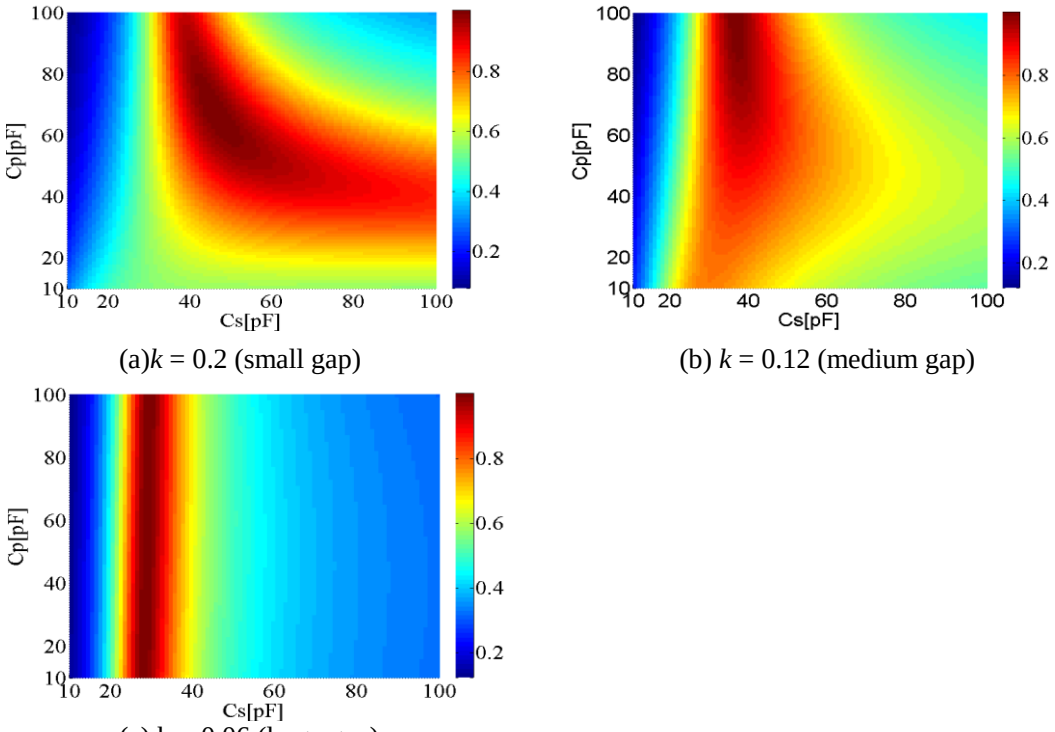

(a)k = 0.2 (small gap) (b) k = 0.12 (medium gap)

(c) k = 0.06 (large gap)

Fig 5.1. Simulation results. S_{21} of the resonators when C_s and C_p are varied. L_s = 5μH in this simulation [19] [32]

Fig 5.1. shows the simulation results of S_{21} in the equivalent circuit in Fig 3.4(a) when the matching parameters (C_s, C_p) are varied from 10 pF to 100 pF. The inductor L_s used in the matching circuit of the simulation is set to be 5000nH, and the coupling coefficient k is varied from 0.05 (large gap) to 0.2 (small gap). Based on the figures, we can observe that there is only a single peak with relatively gentle slopes at strong couplings, and steeper slopes at weaker coupling. This means that almost any optimization algorithm can be used to tune the system as long as the precision of the tuning parameters are sufficiently high. In this case, 1~2 pF for C_s, and 5pF for C_p will be sufficient to accurately tune the system. Another issue that has to be dealt with is the parts where the gradient are too slight as the ratio of the difference in signal as the parameters change becomes too small compared to the noise, increasing the signal to noise ratio. One direct way to solve this problem is by measuring the S_{11} from parameters further apart so that the S_{11} signal difference will be larger.

5.2 Experiment to Validate the Automation of the IM System

With the effect of IM verified, and a simulation to confirm that automation can be easily achievable, an experiment was conducted to validate the automation of the proposed IM system. The prototype IM system proposed in chapter 3.2 and chapter 3.3, and a simple search algorithm based on the Best-Step Steepest Gradient (BSSG) method were used in the experiment. BSSG was used in the experiment to show both the viability and simplicity of the automation of the IM system. In other words, if the BSSG can automate the IM system and maintain maximum efficiency, the choice of search algorithms is very wide, and the potential to improve the speed and robustness of the matching process is huge.

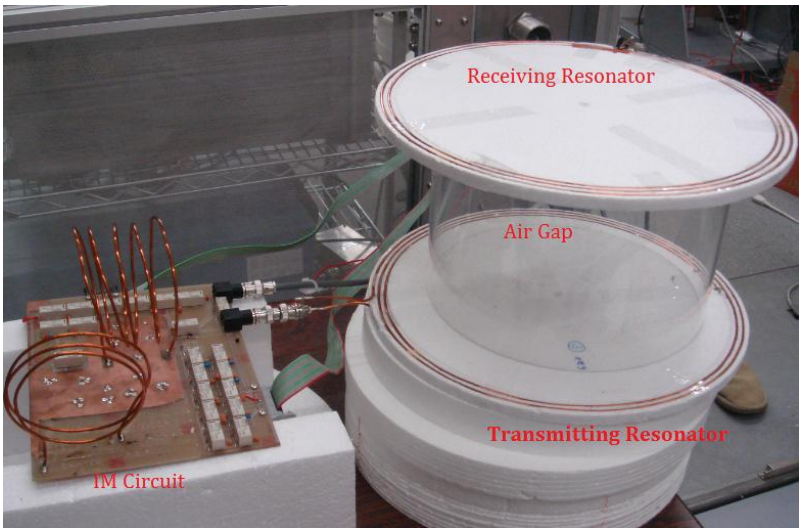

Fig 5.2. Experimental setup for automation experiment with prototype matching circuit.

Fig 5.2 shows a picture of the experimental setup using the prototype matching circuit. This setup is used for the automation experiments in this paper. The experiment is conducted in two steps. First, the proposed system in Fig 3.3. is used along with the IM circuit in Fig 3.8. The attenuator (Fig 3.6) was used as a 50Ω load. The automation was conducted using a PC. The matching process was executed for 3s, and the data of S_{11}, C_s, C_p were recorded. Then, with the final matching parameters unchanged, the power source and attenuator were switched to the VNA to get an accurate measurement of the frequency characteristics. This can be done because both the power source and the attenuator have an impedance of 50Ω, similar to the VNA, thus producing a similar response. Like in the previous chapter, the efficiency of the system is defined as η_{21}. Another advantage of measuring the frequency characteristics is that a more accurate measurement of the reflection ratio can be taken, making it easier to confirm that resonance is occurring.

These experiments are conducted for gap = 6cm ~ 30cm. Experiments for further gaps were not conducted as the results in Fig 4.4 shows that the maximum achievable efficiency for gaps above 30cm is less than 70%, making it not suitable for efficient WPT. While the matching parameters are automated, the matching topography and inducted were pre-selected for these experiments. For gaps 6cm to 20cm, the L-type IM network is used with L_s of approximately 4μH. The inversed L-type IM network is used with L_s of 1.4μH for gaps 21cm to 30cm. The experiments were conducted for 10s.

5.2.1 Best-Step Steepest Gradient (BSSG) Method Search Algorithm

The main objective of the search algorithm is basically to select the matching parameters that will minimize the S_{11} measured by the directional coupler. One of the characteristics of the matching algorithm is that the exact parameters of the function (matching target) is not required, as the output of the function can be experimentally measured. The matching algorithm used in this study uses a classic optimization theory called the steepest gradient method. It finds the local minimum by taking steps proportional to the magnitude of the negative gradient of the function at the current point. When it reaches the local minimum, all gradients from the function at that point will be positive, making the parameters stay at that point. While it is a powerful method to find local minimums, its matching speed is not optimized, and it is very weak towards errors in the measurement of the sensors. The proposed matching algorithm improves on the matching speed and measurement accuracy by scaling the step size taken. It starts with a big step size (10pF), and switches to a smaller step when it reaches its local minimum.

Fig 5.3 shows the flow of the BSSG matching algorithm used in this experiment. The matching process is split into three parts. The initialization (1,2), search loop (3~5), and scaling calculation (6-11).

1. The IM circuit is bypassed (thru), and the S_{11} is measured. If the S_{11} is sufficiently small (<0.2), the IM circuit will remain bypassed (A) as the resonators are already resonating.

2. If S_{11} is bigger than 0.2, the optimization algorithm is initialized before starting the search loop. n represents the loop count of the optimization process. The matching parameters, $\boldsymbol{X}_n=[C_{sn},C_{pn}]^T$ is initialized at $[50pF,50pF]^T$. The vector of the direction of the step used to find the steepest descent $\boldsymbol{D}_n$, size of the step α_n, buffer count used in the step size scaling Buf_n, are initialized at $[0,0]^T$, 10pF, and 0 respectively.
3. When the matching parameters are inserted, S_{11} can be represented as a function of $\boldsymbol{X}_n$. In this step, the S_{11} for $(\boldsymbol{X}_n + \alpha_n\boldsymbol{D}_n)$, where $\boldsymbol{D}_n$ is $[0,0]^T$, $[1,0]^T$, $[-1,0]^T$, $[0,1]^T$, $[0,-1]^T$, is evaluated.
4. The direction with the lowest S_{11} from the five directions mentioned in step 3, $\boldsymbol{D}_{nmin}$ is evaluated.
5. The step which produces the lowest S_{11}, $(\boldsymbol{X}_n + \alpha\boldsymbol{D}_{nmin})$ is chosen as the next matching parameter $\boldsymbol{X}_{n+1}$. The portion of the search algorithm that involves changing the marching parameters ends here.

6 to 11. From step 6 to step 11, a calculation loop is inserted to determine the size of the next step α_{n+1}. There are four possible outcomes from this loop, which are

(a) Path I: (6→7→8→B).

The buffer count Buf_n and step size α_{k+1} of the next loop will remain as it is if the $\boldsymbol{D}_{nmin}$ is not $[0,0]^T$ and $\boldsymbol{D}_{(n-1)min}$ is $[0,0]^T$.

(b) Path II: (6→7→8→11→B).

The next step size α_{n+1} will remain the same but the buffer count Buf_n reinitialized to 0 if $\boldsymbol{D}_{nmin}$ and $\boldsymbol{D}_{(n-1)min}$ is not $[0,0]^T$, and not in the opposite direction of each other.

(c) Path III: (6→9→B).

If $\boldsymbol{D}_{nmin}$ is $[0,0]^T$ or the opposite direction of $\boldsymbol{D}_{(n-1)min}$, the buffer count Buf_n increases by 1 while the step size remains the same.

(d) Path IV: (6→9→10→11→B).

If the conditions in 6(c) are satisfied and Buf_k is larger than the buffer limit (set at 5), Buf_n is reset to 0 and the size of the next step (α_{n+1}) is scaled to half the present size (α_n). This scaling is repeated until α is 1pF to get a higher precision in matching.

Once $\boldsymbol{X}_{n+1}$ and α_{n+1} are determined, the loop returns to step 3 with the newly determined parameters.

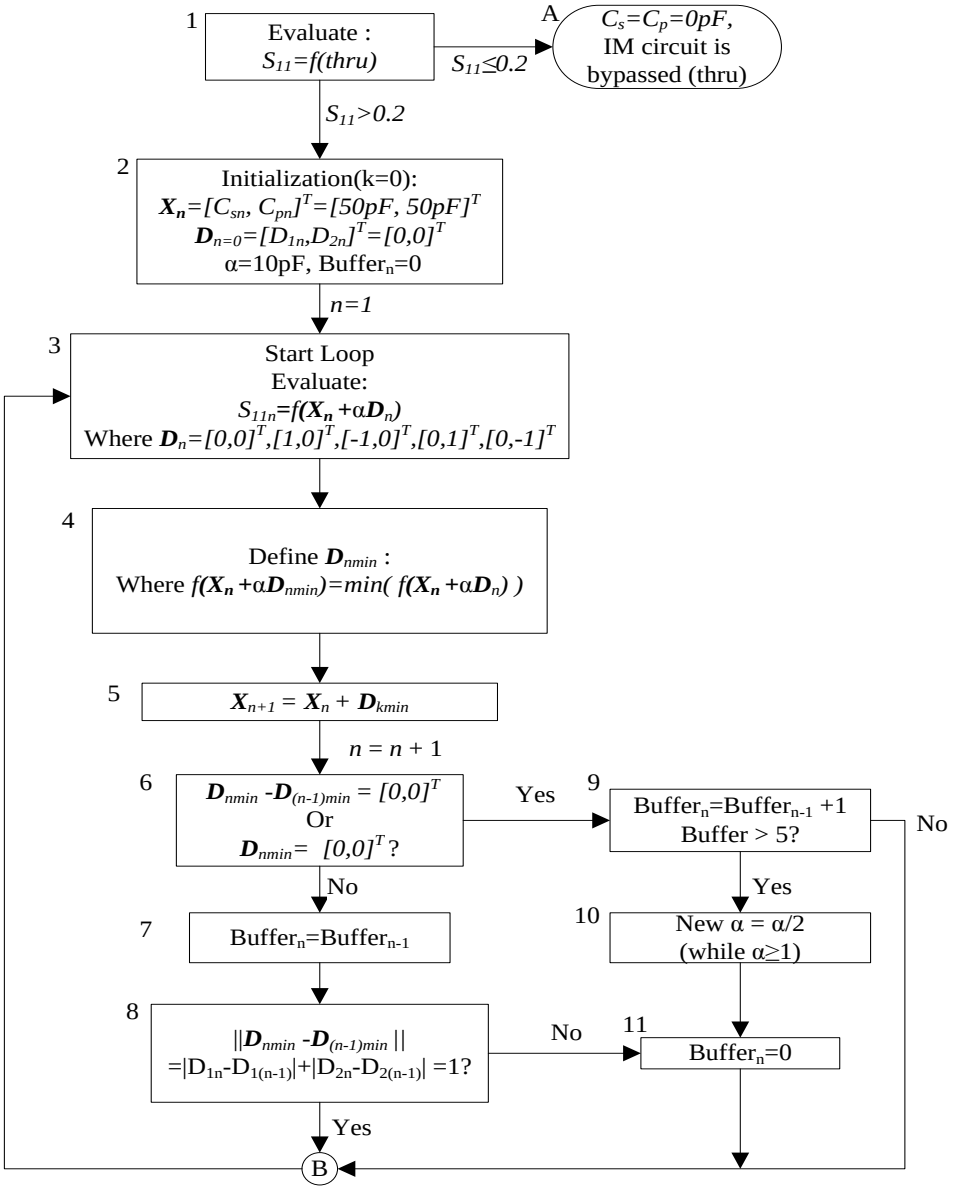

Fig 5.3. Flow chart of the BSSG matching algorithm used in the experiment

5.2.2 Experimental Results of Automation Validation Experiment

Fig 5.4 shows the efficiency versus gap graph of the BSSG automation experiment. *After (Manual, Ideal)* can be considered the maximum efficiency that can be achieved as the size of the circuit is minimized, reducing all possible losses through ohm loss and stray reactance. The results show that the efficiency of the proposed IM circuit *After (Auto, BSSG)* can reach 85%, only 5% lower than the ideal case *After (Manual, Ideal)*. The 5% loss is mainly due to the ohm loss caused by the bigger size of the automated IM circuit used in the automation experiments (Fig 3.8). Moreover, by increasing the efficiency of the system, the IM circuit also increased the range where energy can be transmitted at maximum efficiency.

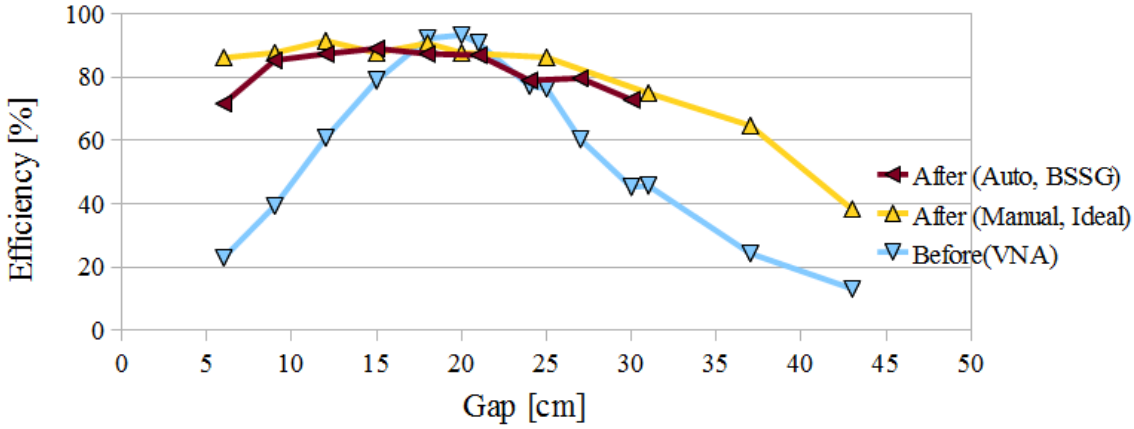

Fig 5.4. Experimental results. Efficiency vs gap graph of WPT using proposed BSSG automated impedance matching system. Here, L-type IM network is used for gaps 6cm to 20cm, and the Inversed L-type IM network is used for gaps 21cm to 43cm.
Before(VNA) represents the efficiency of the resonators without the IM circuit. *After (Manual, Ideal)* represents the efficiency of the system after it is manually matched using the method and circuit introduced in *Chapter 4* (Fig 4.3). *After (Auto, BSSG)* is the efficiency of the system after it is automatically matched using the system proposed in Chapter 3 (Fig. 3.3 to Fig 3.8) with the BSSG.

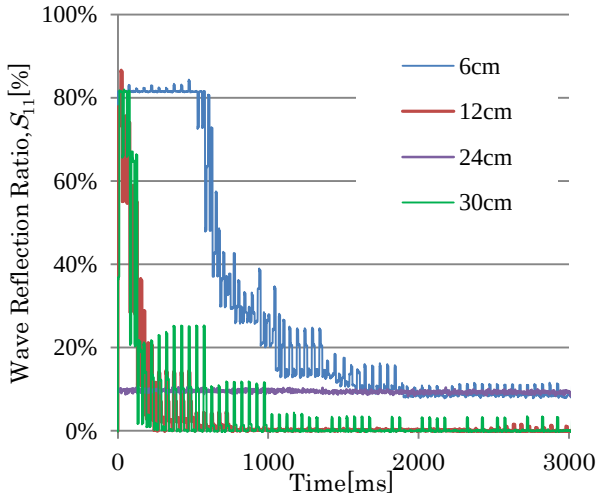

Fig 5.5 Experimental results. S_{11} versus time graph of automated IM matching using BSSG. Results got Gap = 6cm, 12cm, 24cm and 30cm were chosen to represent the typical time response of S_{11}..

Fig 5.5 shows the typical S_{11} vs time graph of automated IM matching using BSSG, and Fig 5.6 shows the detailed results of the frequency characteristics, S_{11} vs time, and matching parameters vs time graph. Only the results up to 3s are shown as all experiments stabilized by then. Fig 5.5(a)~(e) and Fig 5.5 (h)~(i) shows the response of the experiments on the L-type and inverted L-type matching network respectively, while Fig 5.5(f)(g) shows the results when the IM circuit is bypassed. The results here verify that efficiency is increased by matching the resonators as in Chapter 4. This can be confirmed by noting that the S_{11} at 13.56MHz is very low, almost zero in most cases. As the

IM circuit is bypassed in 21cm and 24cm, the frequency characteristic does not significantly change. The 5% increase in efficiency of 24cm gap in Fig 5.3 is not due to the matching process, but the change in frequency characteristics when the IM circuit is inserted before the transmitting resonator.

The S_{11} vs time results in Fig 5.4 shows that the system generally takes 0.25s to 1s to reach a wave reflection ratio of less than 10%, and it takes up to 1.5s to completely settle. The results show that the simple BSSG algorithm tested can decrease the S_{11} to less than 10%, meaning the reflected power η_{11} is reduced to less than 1% (from equation (2-5)). This means that all the resonators were successfully matched. While the S_{11} for most experiments ended at almost 0%, the experiments for 6cm and 24cm show a final of approximately 8%. The S_{11} for 24cm stop at 8% because the IM circuit is bypassed as the reflection ratio is evaluated to be sufficient low. On the other hand, the result in the 6cm experiment could be due to the error in the S_{11} sensor reading caused by the non-linearity and the cutoff voltage of the diode used to rectify the AC signal from the directional coupler. (Note that the S_{11} reading at the computer's AD board is slightly different from that of the directional coupler due to the non-linearity and cutoff voltage of the diode.) This problem can be solved by improving the analog circuit used as the rectifier for the AD input, and enhancing the search algorithm.

Even with a simple matching algorithm that is not optimized for speed, the matching time is still significantly higher than regular IM systems that use variable condensers that are controlled by motors due to the fast switching speeds of the relays and the fast response of the 13.56MHz system. The matching speed is an important factor when dealing with moving objects and changing loads. To cope with these fast changing impedances, a more sophisticated matching control need to be applied. The options include improving the optimization search algorithm [24]- [27], and measuring the voltage and current at the transmission resonator to calculate the impedance so that a better set of initial parameters can be chosen.

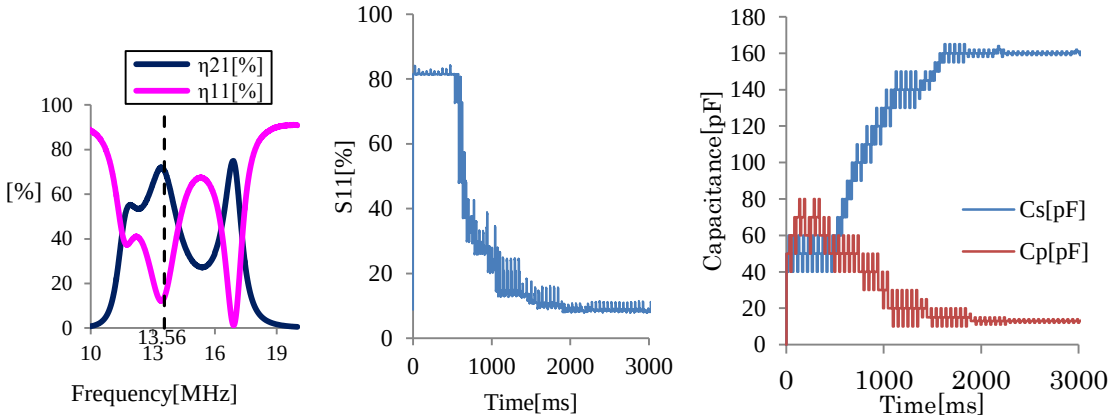

(i) Frequency Characteristics (ii) S_{11} vs Time (iii) Matching parameters vs Time

(a) Gap = 6cm, L-matching circuit and L_s = 4μH

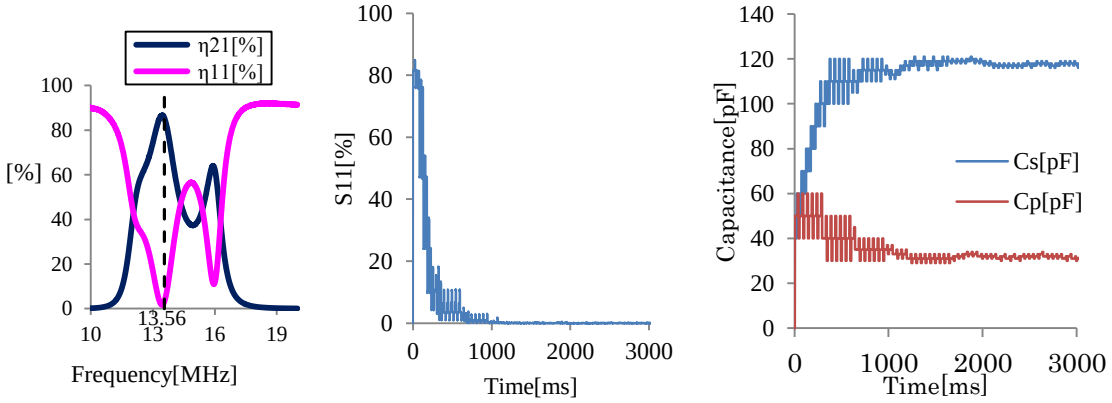

(i) Frequency Characteristics (ii) S_{11} vs Time (iii) Matching parameters vs Time

(b) Gap = 9cm, L-matching circuit and L_s = 4μH

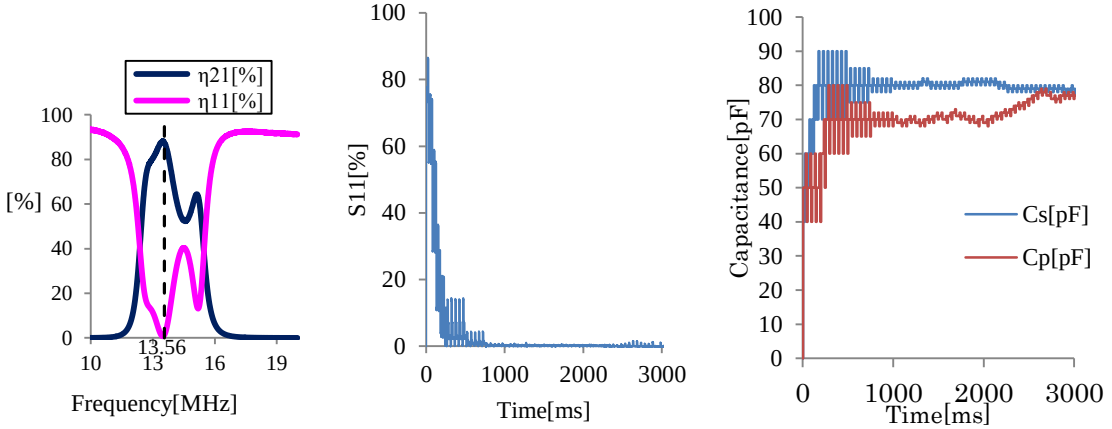

(i) Frequency Characteristics (ii) S_{11} vs Time (iii) Matching parameters vs Time

(c) Gap = 12cm, L-matching circuit and L_s = 4μH

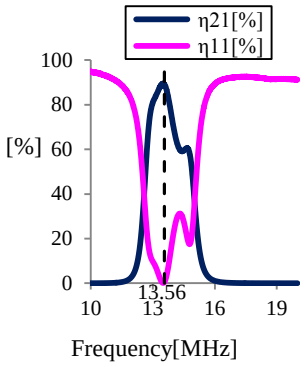

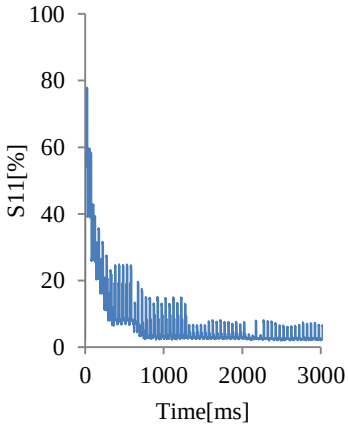

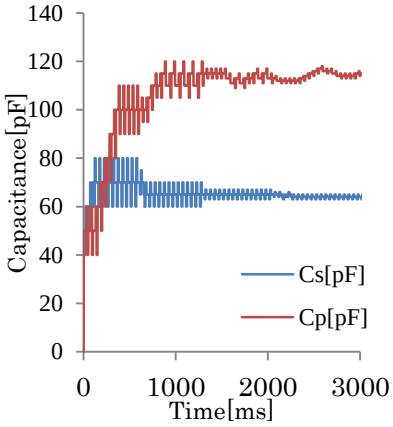

(i) Frequency Characteristics (ii) S_{11} vs Time (iii) Matching parameters vs Time

(d) Gap = 15cm, L-matching circuit and L_s = 4μH

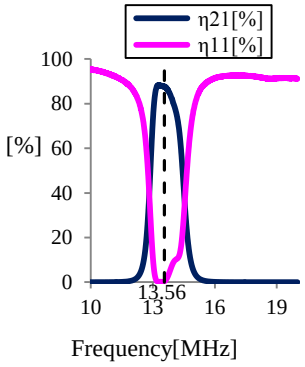

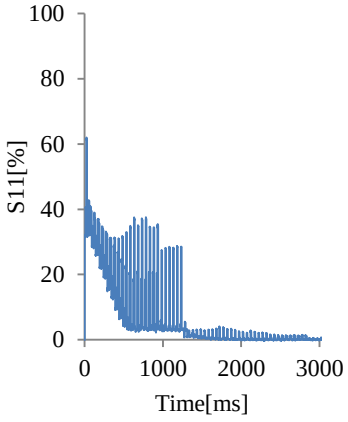

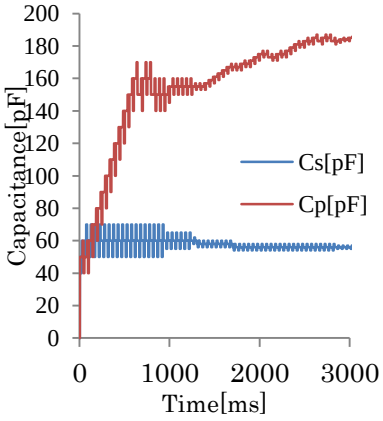

(i) Frequency Characteristics (ii) S_{11} vs Time (iii) Matching parameters vs Time

(e) Gap = 18cm, L-matching circuit and L_s = 4μH

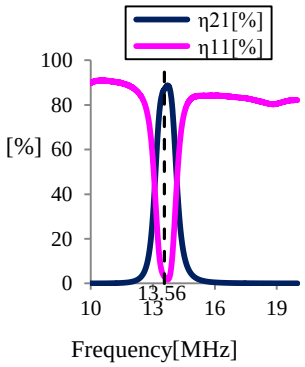

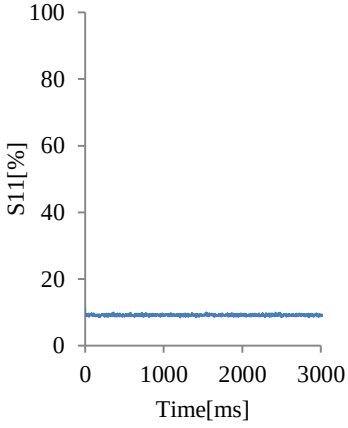

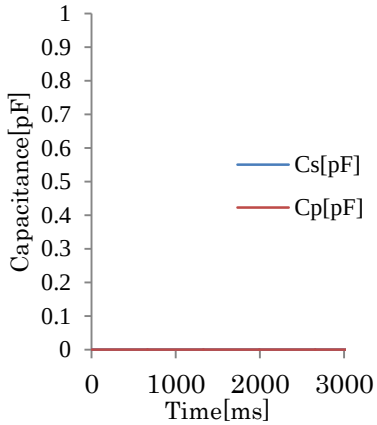

(j) Frequency Characteristics (ii) S_{11} vs Time (iii) Matching parameters vs Time

(f) Gap = 21cm, Matching circuit bypassed (thru)

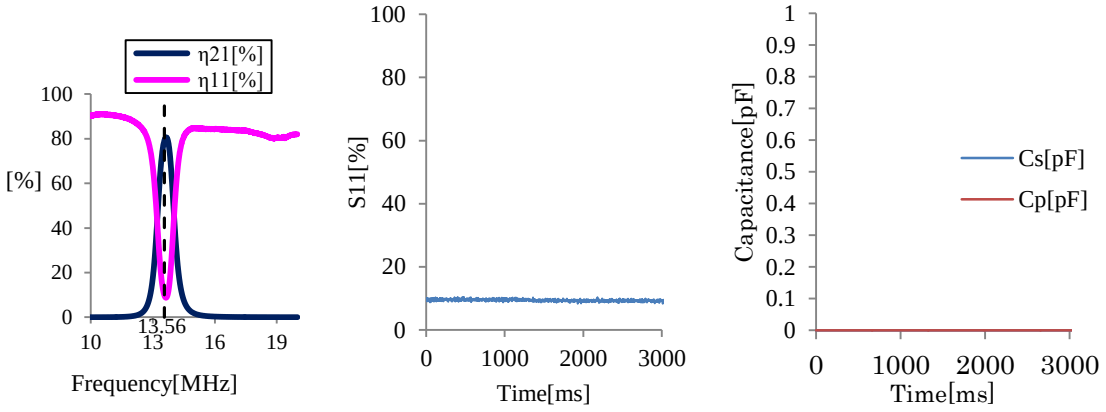

(k) Frequency Characteristics (ii) S_{11} vs Time (iii) Matching parameters vs Time

(g) Gap = 24cm, Matching circuit bypassed (thru)

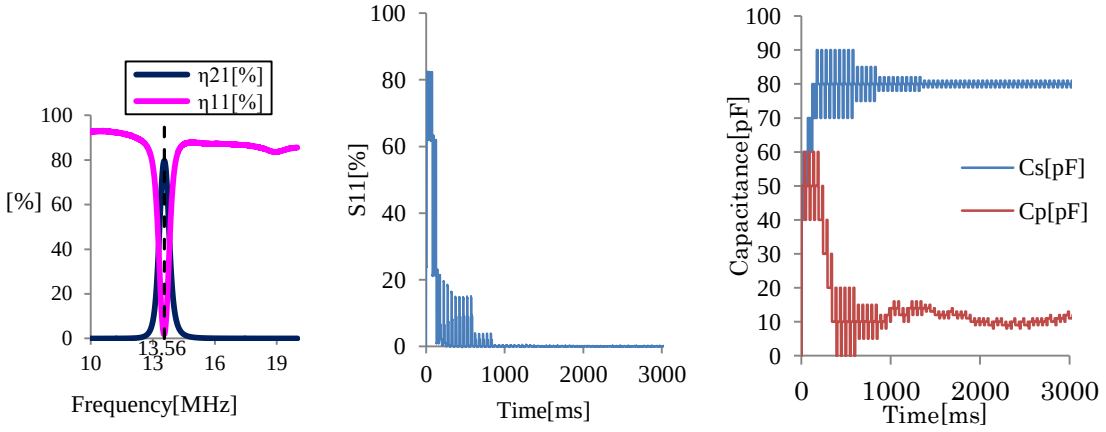

(l) Frequency Characteristics (ii) S_{11} vs Time (iii) Matching parameters vs Time

(h) Gap = 27cm, Inversed L-matching and L_s = 1.4μH

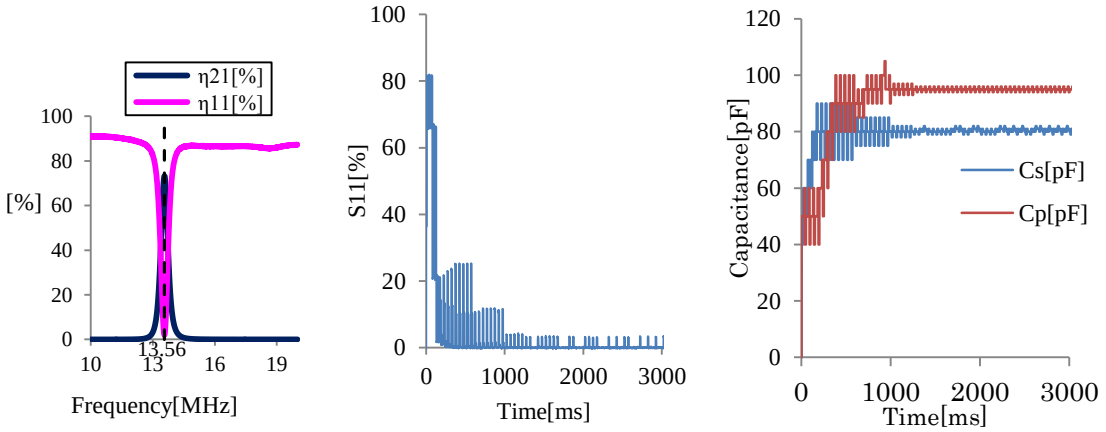

(m) Frequency Characteristics (ii) S_{11} vs Time (iii) Matching parameters vs Time

(i) Gap = 30cm, Inversed L-matching and L_s = 1.4μH

Fig 5.6. Experimental results of WPT with proposed automated IM system using BSSG. Frequency characteristics after matching, and S_{11} and matching parameters vs time graphs of the matching process. Matching topography and L_s is preselected for this experiment.

5.3 Summary

In a nutshell, this chapter verified that the proposed IM circuit can be automated to increase the efficiency and extend the range of the MRC wireless power transfer system. The experiment results show that the efficiency can be increased to up to 85% (almost ideal) within 0.5s to 1.5s. a simple Best-Step Steepest Gradient method search algorithm. IT shows that automation can be easily achieved to make the system more robust towards changes in the gap and displacement of the receiving resonator.

The system that uses only a directional coupler to measure the reflected wave ratio at the transmitting end of the system, and high frequency relays to select the matching parameters needed to minimize the reflected wave. The IM circuit used is made of high Q-value air-core coils and ceramic condensers, and placed on a Printed Circuit Board (PCB).

Chapter 6 Improved Automated IM System Using Golden Section Search (GSS) Algorithm

In the previous chapters, the prototype IM circuit made on PCB was introduced, and a BSSG based matching algorithm was used to automate the system. While the proposed hardware could achieve high efficiency (85%) after matching, the matching time is 0.5s to 2.0s, leaving space for improvement. This chapter focuses on the search algorithm to study the achievable matching time with the proposed setup that uses only the feedback from the directional coupler and high frequency relays to select the parameters. A two-dimensional Golden Section Search (GSS) technique is introduced to improve the matching speed of the system. Its effect are studied with experiments for both stationary and moving receivers. The experimental setup and methodology is the same as the experiment described in Chapter 5. The only difference is the matching algorithm used, and the length of experiment that is reduced to 1s (from 10s).

6.1 Proposed GSS Algorithm

As mentioned in Chapter 3 and Chapter 5, the IM system involves selecting two parameters (C_s,C_p) to reduce the S_{11} measured by the directional coupler. Therefore it can be solved as a two dimension minimization problem. In this chapter, the GSS is proposed as a search algorithm to achieve a fast and precise matching. The GSS is closely related to the Fibonacci Search, [27] [33] which is widely considered an industrial process. The performance of the process is measured in terms of a function $f(\boldsymbol{x})$, which is evaluated experimentally. The main advantage that GSS has over Fibonacci Search is that the GSS does not require a Priori, the number of evaluations to satisfy the minimum search process. For the GSS to be successful, the following conditions must be satisfied.

- The functions $f(\boldsymbol{x})$ is unimodal. This means that it has only one global minimum point (valley) and no local peaks/valleys.
- The optimum (minimum in this case) point of $f(\boldsymbol{x})$ is located within an interval $\boldsymbol{x}_{gsmin} \leqq \boldsymbol{x} \leqq \boldsymbol{x}_{gsmax}$, but each test point that is checked expends a certain amount of time and performance.

The simulation results in Fig 5.1 and the experimental results in Chapter 5.2.2. shows that the matching parameter with maximum efficiency is unimodal, thus it satisfies the first condition for GSS. However, the matching control has two controllable variables. To satisfy the second condition and apply the GSS to this IM system, the search algorithm is separated into three compartments, namely the Direction Selection Loop, Bracketing Loop and Golden Section Search Loop.

TABLE II :

Definitions in GSS Matching Algorithm

A	Direction search step size	
B	Bracketing step size	
n, Br, Gss	Loop counter for overall search loop, bracketing loop and golden search ratio loop respectively	
$\boldsymbol{X}$	Matching parameters	$\boldsymbol{X} = \begin{bmatrix} C_\mathrm{s} \\ C_\mathrm{p} \end{bmatrix}$
$\boldsymbol{D}$	Direction vector	$\boldsymbol{D} = \begin{bmatrix} \mathrm{d_s} \\ \mathrm{d_p} \end{bmatrix}$
S_{11}	Measured reflection wave ratio	$S_{11} = \mathrm{f}(\boldsymbol{X}_\mathrm{n}) = \mathrm{f}(\begin{bmatrix} C_\mathrm{s} \\ C_\mathrm{p} \end{bmatrix})$
$\Delta f(\boldsymbol{X}_\mathrm{n})_{\alpha,\mathrm{D}}$		$\Delta\mathrm{f}(\boldsymbol{X}_\mathrm{n})_{\alpha,\mathbf{D}} = \mathrm{f}(\boldsymbol{X}_\mathrm{n} + \propto \boldsymbol{D}) - \mathrm{f}(\boldsymbol{X}_\mathrm{n})$
$\boldsymbol{D}_\mathrm{min}$	Direction vector with lowest S_{11}	Define $\boldsymbol{D}_\mathrm{min}$ Where $\Delta\mathrm{f}(\boldsymbol{X}_\mathrm{n})_{\alpha,\mathbf{D}_\mathrm{min}} = \min \Delta\mathrm{f}(\boldsymbol{X}_\mathrm{n})_{\alpha,\mathbf{D}}$ Where $\mathbf{D} = \begin{bmatrix} 0 \\ 0 \end{bmatrix}, \begin{bmatrix} 1 \\ 0 \end{bmatrix}, \begin{bmatrix} -1 \\ 0 \end{bmatrix}, \begin{bmatrix} 0 \\ 1 \end{bmatrix}, \begin{bmatrix} 0 \\ -1 \end{bmatrix}$
$\boldsymbol{D}_\mathrm{smin}$	Direction vector for C_s with lowest S_{11}	Define $\boldsymbol{D}_\mathrm{smin}$ Where $\Delta\mathrm{f}(\boldsymbol{X}_\mathrm{n})_{\alpha,\mathbf{D}_\mathrm{smin}} = \min \Delta\mathrm{f}(\boldsymbol{X}_\mathrm{n})_{\alpha,\mathbf{D}}$ Where $\mathbf{D} = \begin{bmatrix} 1 \\ 0 \end{bmatrix}, \begin{bmatrix} -1 \\ 0 \end{bmatrix}$
$\boldsymbol{D}_\mathrm{pmin}$	Direction vector for C_p with lowest S_{11}	Define $\boldsymbol{D}_\mathrm{min}$ Where $\Delta\mathrm{f}(\boldsymbol{X}_\mathrm{n})_{\alpha,\mathbf{D}_\mathrm{min}} = \min \Delta\mathrm{f}(\boldsymbol{X}_\mathrm{n})_{\alpha,\mathbf{D}}$ Where $\mathbf{D} = \begin{bmatrix} 0 \\ 1 \end{bmatrix}, \begin{bmatrix} 0 \\ -1 \end{bmatrix}$
r_S	Ratio of C_s step size	$r_\mathrm{s} = \frac{\left\lvert \Delta\mathrm{f}(\boldsymbol{X}_\mathrm{n})_{\alpha,\mathbf{D}_\mathrm{smin}} \right\rvert}{\left\lvert \Delta\mathrm{f}(\boldsymbol{X}_\mathrm{n})_{\alpha,\mathbf{D}_\mathrm{smin}} \right\rvert + \left\lvert \Delta\mathrm{f}(\boldsymbol{X}_\mathrm{n})_{\alpha,\mathbf{D}_\mathrm{pmin}} \right\rvert}$
r_p	Ratio of C_p step size	$r_\mathrm{p} = \frac{\left\lvert \Delta\mathrm{f}(\boldsymbol{X}_\mathrm{n})_{\alpha,\mathbf{D}_\mathrm{pmin}} \right\rvert}{\left\lvert \Delta\mathrm{f}(\boldsymbol{X}_\mathrm{n})_{\alpha,\mathbf{D}_\mathrm{smin}} \right\rvert + \left\lvert \Delta\mathrm{f}(\boldsymbol{X}_\mathrm{n})_{\alpha,\mathbf{D}_\mathrm{pmin}} \right\rvert}$
D_search	Direction for 1-dimensional search for Bracketing and GSS	(Method 1: Scalar Search): $\boldsymbol{D}_\mathrm{search} = \boldsymbol{D}_\mathrm{min}$ (Method 2: Vector Search): $\boldsymbol{D}_\mathrm{search} = r_\mathrm{s}\boldsymbol{D}_\mathrm{smin} + r_\mathrm{p}\boldsymbol{D}_\mathrm{pmin}$

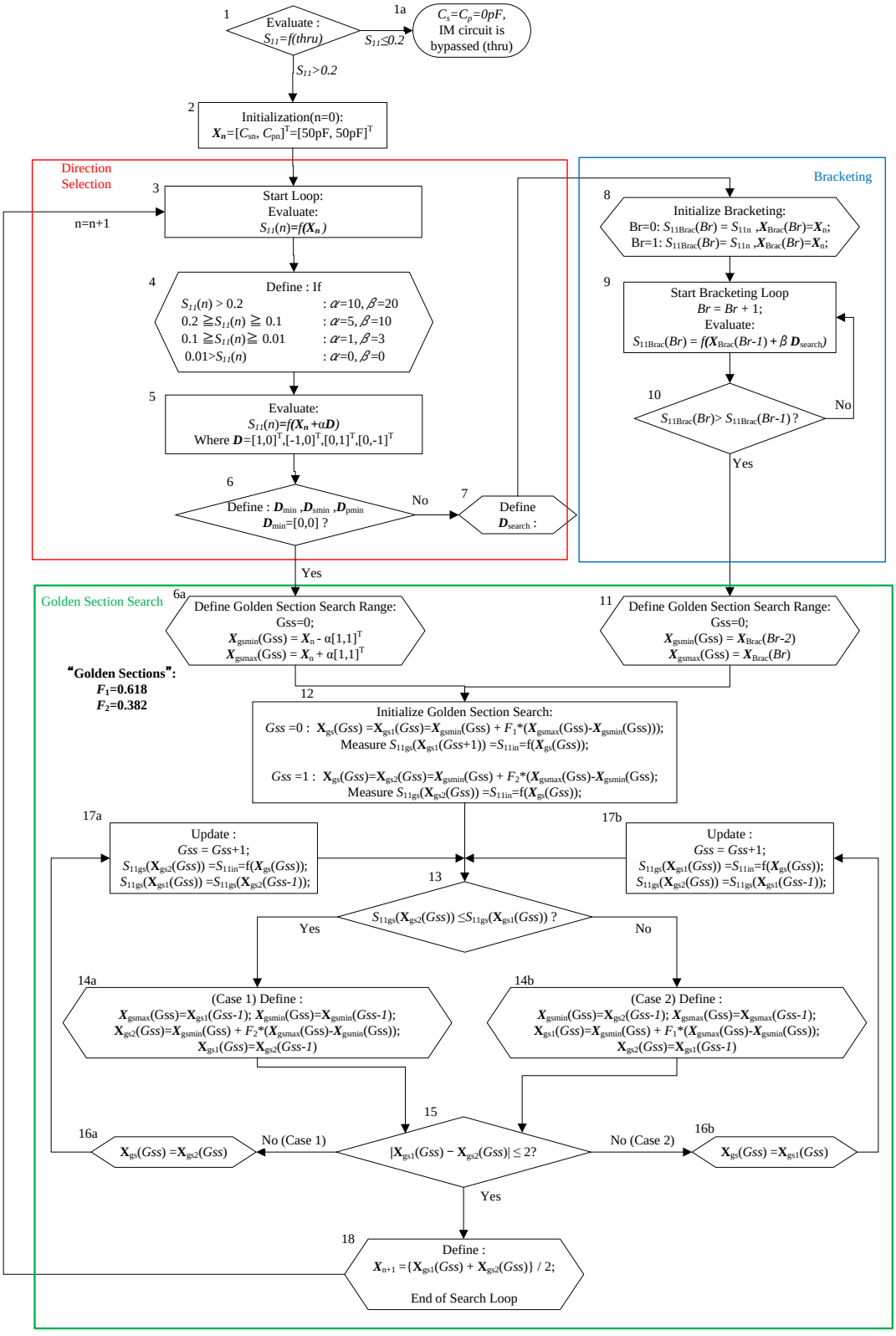

Fig 6.1. Flowchart of the S_{11} minimization algorithm based on the Golden Section Search technique

Fig 6.1 is the flow of the search algorithm with mathematical expressions. The definitions of the variables used in the matching algorithm are shown in TABLE II. The algorithm starts by measuring the S_{11} when the IM circuit is bypassed (step 1), and IM will be to (C_s,C_p)=(50pF,50pF) and initialized if the S_{11} reading is above 0.2 (step 2). Then the search loop begins, and it is separated into the following three main parts.

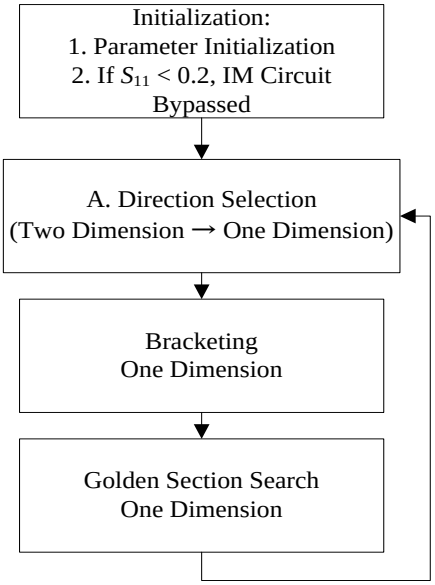

Fig 6.2. Overall flow of the proposed algorithm. (Simplified)

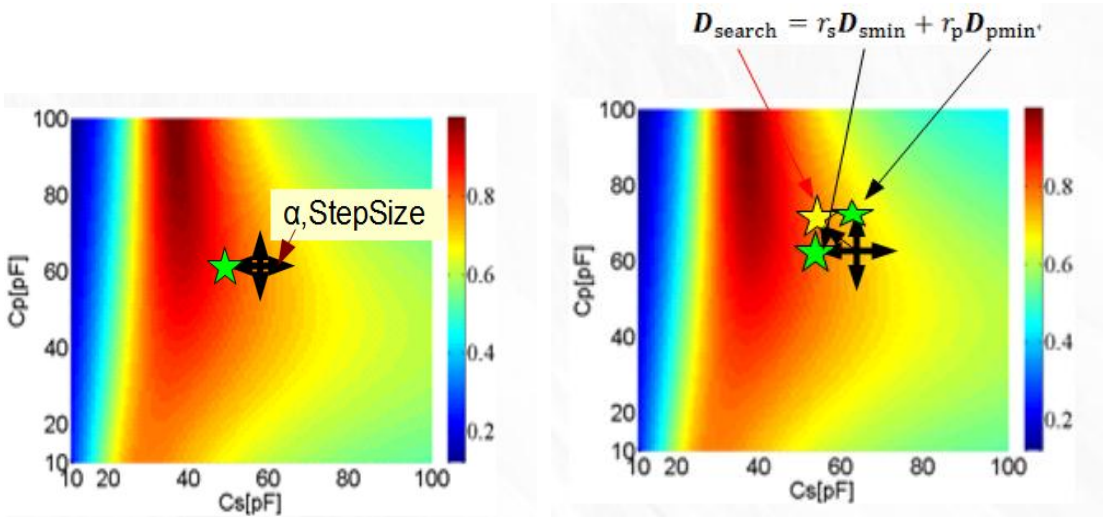

(a) Scalar GSS (b) Vector GSS

Fig 6.3. Pictorial expression of the Direction Selection Search Loop. (Simplified) The green star represents the direction of the axis with the steepest descent, and the yellow star is the vector whose ratio of each axis is proportional to the gradient.

A) Direction Selection (Steps 3 to 7) – Selects the direction to perform the bracketing and GSS according to the S_{11} of the current matching parameter $[C_{sn}\ C_{pn}]^T$ and its surrounding parameters, $[C_{sn} \pm\alpha,\ C_{pn}\pm\alpha]^T$, and selects the direction for the next two loops, changing the two dimension problem into a one dimension problem. The size of the step in this section, α is determined by the S_{11} at $[C_{sn}\ C_{pn}]^T$. Two methods are tested in the Direction Selection Loop, called the Scalar GSS and Vector GSS respectively. Fig 6.3 shows the pictorial expression of the Direction Selection Loop to help improve understanding. The Scalar GSS simply takes the direction where the decent of S_{11} is the steepest, just like the best-step steepest gradient method, and performs the bracketing and GSS. It is very similar to typical IM systems where one parameter is used for rough tuning, and the other parameter for fine tuning. On the other hand, the Vector GSS is the common multidimensional GSS technique where the ratio of the step of each dimension is proportional to the gradient of their descent. According to Fig 5.1, the C_s parameter can be used for rough tuning while the C_p parameter can be used for fine tuning. Given that the bracketing sizes β are the same, the Scalar-GSS can potentially reach a low S_{11} point faster than the Vector GSS. Contrarily, Vector GSS can approach the valley (optimal point) faster than the Scalar CSS. In this case, the first overall loop will function as the rough tuning, and the second overall loop will function as the fine tuning.

3. The search loop starts by evaluating the S_{11} of the previously selected matching parameters, $\boldsymbol{X}_n$.
4. The step size of the direction search loop, α,and the bracketing loop β, is determined according to the measured S_{11} value as in TABLE II. The main reason behind this is to have the optimum signal-to-noise ratio of the S_{11} readings while keeping the smallest step size for α, and to keep the bracketing loop to a small value.
5. After that, the S_{11} for the surrounding parameters are also measured.
6. The direction of the matching parameter with the lowest S_{11} reading, $\boldsymbol{D}_{min}$ is calculated. If all surrounding matching parameters have higher S_{11} reading than $\boldsymbol{X}_n$, the GSS is activated with $[C_{sn}\text{-}\alpha,\ C_{pn}\text{-}\alpha]^T$ and $[C_{sn}+\alpha,\ C_{pn}+\alpha]^T$ as the minimum and maximum of the initial matching parameter search range, $\boldsymbol{X}_{gsmin}(0)$ and $\boldsymbol{X}_{gsmax}(0)$ respectively. (step 6a) This step is to prevent the search algorithm from staying at a single point away from the optimum point because the gradient near the valley was so sharp that the surrounding parameters α steps away show a higher S_{11} reading than $\boldsymbol{X}_n$. Otherwise, the direction for both C_s and C_p which has the lowest S_{11} reading is calculated.
7. Finally, the direction for the one-dimensional search loops (bracketing and GSS) are decided according to the two methods mentioned above. (TABLE II)

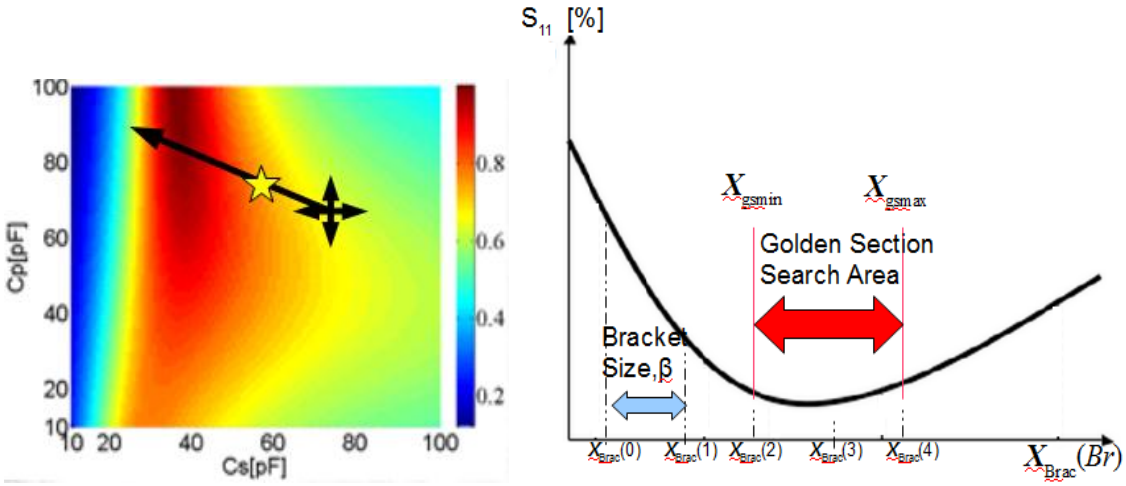

(a) Bracketing direction in 2-D (b) Bracketing process in 1-D

Fig 6.4. Pictorial expression of the Bracketing Loop. (Simplified)(Modified from google images)

B) Bracketing (Steps 8 to 10) – Selects the range at which the GRO is performed. Once the direction is determined (Fig 6.4(a)), the C_s and C_p will be swept at large bracketing steps, β, until the S_{11} in larger than that of the previous steps. When this happens, the minimum and maximum value of the search range for GSS is determined. (Fig 6.4(b))

8. The bracketing loop is initialized by defining the initial two sets (Br=0,1) of matching parameters $\boldsymbol{X}_{\mathrm{Brac}}(Br)$ and their S_{11} value ($S_{11\mathrm{Brac}}(Br)$) as $\boldsymbol{X}_{\mathrm{n}}$ and $S_{11\mathrm{n}}$ respectively. This is merely for convenience in case the next bracketing step shows a higher reading of S_{11} than $S_{11\mathrm{n}}$.
9. The S_{11} of the next bracketing parameter with a step size of β($S_{11\mathrm{Brac}}(Br) = f(\boldsymbol{X}_{\mathrm{Brac}}(Br\text{-}1) + \beta\boldsymbol{D}_{\mathrm{search}})$) is measured.
10. If the reading is lower than that of the previous bracketing parameter, the search loop is repeated. Otherwise, the minimum and maximum value of the search range for GSS is determined.

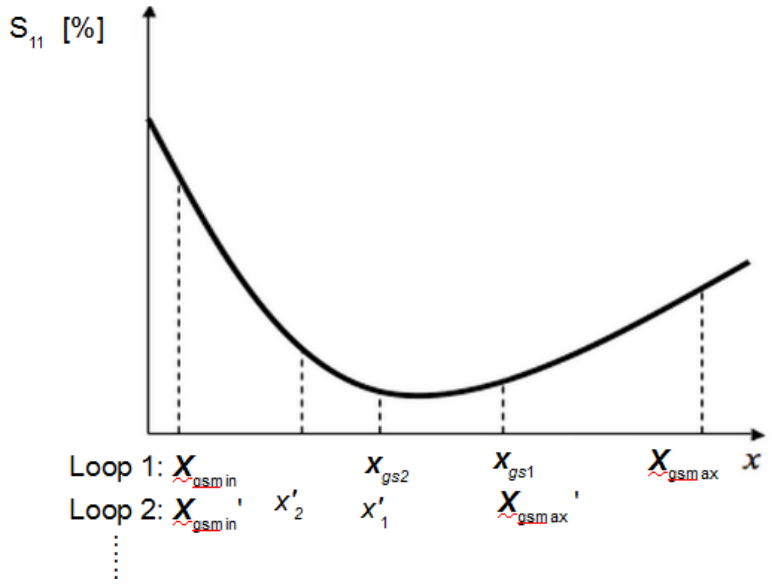

Fig 6.5. Pictorial expression of the GSS Loop. (Simplified)(Modified from google images)

C) Golden Section Search (Steps 11 to 18) – Once the search range of the GSS is determined through bracketing, the GSS loop can be implemented, and the S_{11} of the parameters between the search range is sampled according to the golden sections, F_1 and F_2. (F_1 = 0.618, F_2 = 0.382)[27]. (Fig 6.5) The direction of the GSS search is the same as the one used for bracketing, $\boldsymbol{D}_{\text{search}}$.

11. The minimum and maximum of the initial matching parameter search range, $\boldsymbol{X}_{\text{gsmin}}(0)$ and $\boldsymbol{X}_{\text{gsmax}}(0)$ is defined as $\boldsymbol{X}_{\text{brac}}(Br\text{-}2)$ and $\boldsymbol{X}_{\text{brac}}(Br)$ respectively. These are the third and furthest points of the bracketing loop. It is defined this way because this is the point where the S_{11} value rise, meaning the matching parameter with the minimum S_{11} is in between these two numbers.
12. The GSS is initialized by calculating the two values of matching parameters $\boldsymbol{X}_{\text{gs1}}$ and $\boldsymbol{X}_{\text{gs2}}$ in the interval $<\boldsymbol{X}_{\text{gsmin}}, \boldsymbol{X}_{\text{gsmax}}>$ using the golden sections. The S_{11} values corresponding to these two parameters $S_{11\text{gs}}(\boldsymbol{X}_{\text{gs1}})$ and $S_{11\text{gs}}(\boldsymbol{X}_{\text{gs2}})$ are measured accordingly.
13. This step compares the two S_{11} readings and determines the next step.
14. Depending on the comparisons in step 13, step 14a or 14b are executed, where the interval $<\boldsymbol{X}_{\text{gsmin}}, \boldsymbol{X}_{\text{gsmax}}>$ is reduced and the new values ($\boldsymbol{X}_{\text{gs1}}$ and $\boldsymbol{X}_{\text{gs2}}$) of the newly updated interval $<\boldsymbol{X}_{\text{gsmin}}, \boldsymbol{X}_{\text{gsmax}}>$ is recalculated.
15. The corresponding S_{11} values of the new $\boldsymbol{X}_{\text{gs1}}$ and $\boldsymbol{X}_{\text{gs2}}$ are re-measured and re-evaluated (Step 16,17) until the desired accuracy is met. In this paper, the GSS loop stops when the interval between $\boldsymbol{X}_{\text{gs1}}$ and $\boldsymbol{X}_{\text{gs2}}$ is less than 2, and the next matching parameter $\boldsymbol{X}_{\text{n}}$ is defines as the average of $\boldsymbol{X}_{\text{gs1}}$ and $\boldsymbol{X}_{\text{gs2}}$.(Step 18)

This GSS based search algorithm is used in the experiment to determine the matching parameters X, but the matching topography and L values are pre-selected. In this paper, the topography is set at L and L_1=4.8μH when the gap is less than 20cm and inverted-L and L_1=1.4μH when it is bigger than 20cm.

6.2 Experimental Results of Proposed GSS Algorithm

Fig 6.6 shows the efficiency versus gap graph of different matching algorithms. The top three data series shown in the legend is the final efficiency of the system after it is automatically matched using the prototype PCB made IM circuit using the Scalar GSS, Vector GSS and BSSG respectively. The yellow line *After (Manual, Ideal)* is the efficiency of the system after it is manually matched using ceramic condensers as in Chapter 4, and *Before (VNA)* is the efficiency of the resonator pair without an IM circuit. The results show that the proposed GSS automated system can achieve a high efficiency of 80~85% (for Vector GSS). As in Chapter 5, the 5% efficiency loss compared to the ideal result (90%) is due to the larger IM circuit which causes more ohm loss and stray capacitance. Furthermore, both GSS results in generally the same final efficiency, with the Vector GSS slightly higher in a few cases. This can be because the vector search will naturally reach a point closer to the minimum point in the first search loop, while the scalar search might potentially stop after the first overall loop (rough tuning) as the difference in S_{11} after that point is not significant enough compared to the noise.

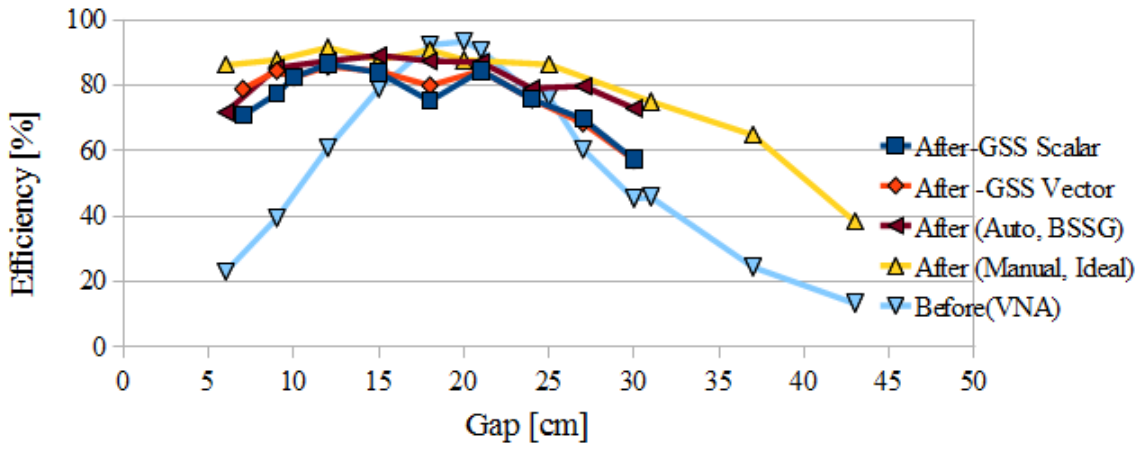

Fig 6.6. Experimental results. Efficiency vs gap graph of WPT using proposed BSSG automated impedance matching system. Here, L-type IM network is used for gaps 6cm to 20cm, and the Inversed L-type IM network is used for gaps 21cm to 43cm.

Before(VNA) represents the efficiency of the resonators without the IM circuit. *After (Manual, Ideal)* represents the efficiency of the system after it is manually matched using the method and circuit introduced in *Chapter 4* (Fig 4.3). *After –GSS Scalar*, *After –GSs Vector* and *After (Auto, BSSG)* is the efficiency of the system after it is automatically matched using the system proposed in Chapter 3 (Fig. 3.3 to Fig 3.8) with the Scalar and Vector GSS, and BSSG respectively.

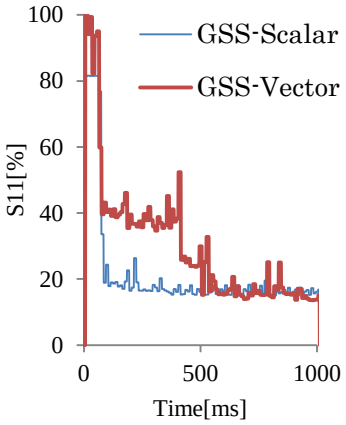

(i) S_{11} vs Time

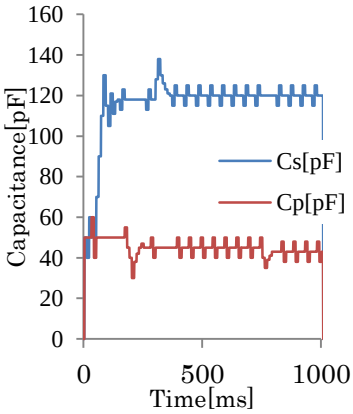

(ii) (C_s,C_p) vs Time
GSS-Scalar

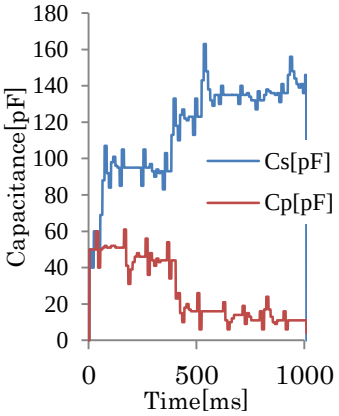

(iii) (C_s,C_p) vs Time
GSS-Vector

(a) Gap = 7cm, L-matching circuit and L_s = 4μH

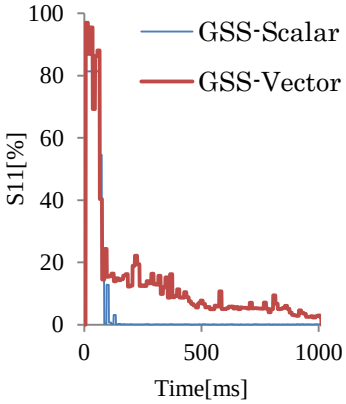

(i) S_{11} vs Time

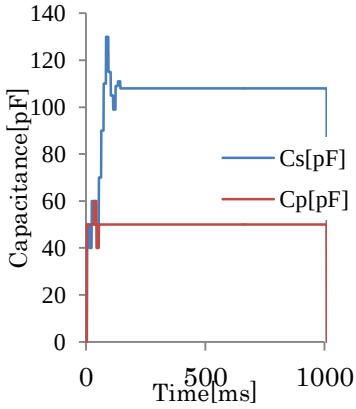

(ii) (C_s,C_p) vs Time
GSS-Scalar

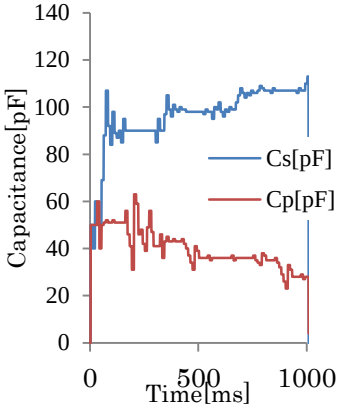

(iii) (C_s,C_p) vs Time
GSS-Vector

(b) Gap = 9cm, L-matching circuit and L_s = 4μH

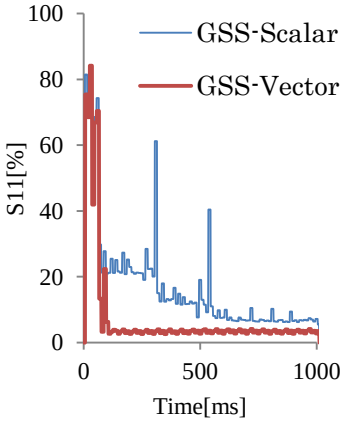

(i) S_{11} vs Time

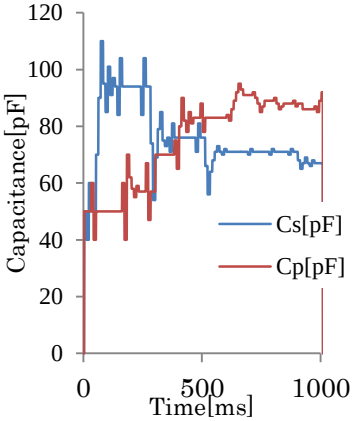

(ii) (C_s,C_p) vs Time
GSS-Scalar

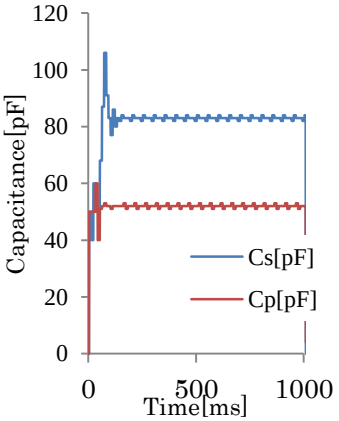

(iii) (C_s,C_p) vs Time
GSS-Vector

(c) Gap = 12cm, L-matching circuit and L_s = 4μH

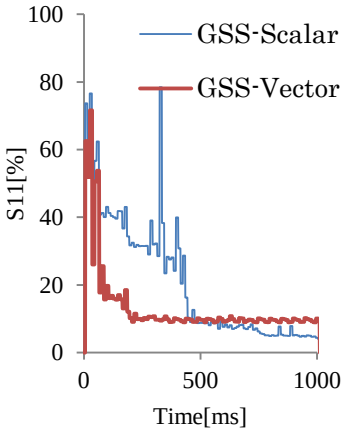

(i) S_{11} vs Time

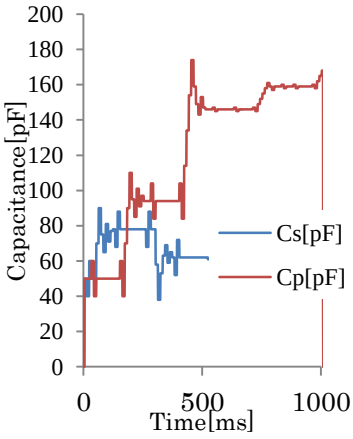

(ii) (C_s,C_p) vs Time GSS-Scalar

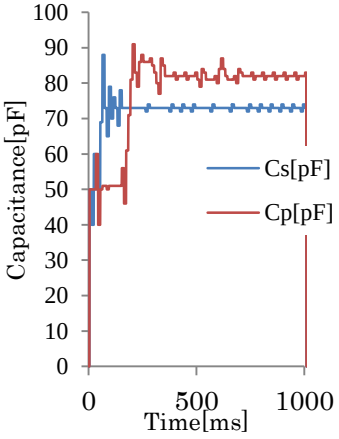

(iii) (C_s,C_p) vs Time GSS-Vector

(d) Gap = 15cm, L-matching circuit and L_s = 4μH

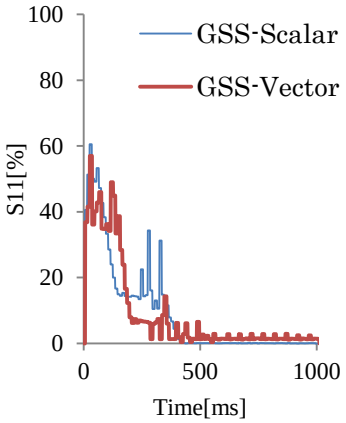

(i) S_{11} vs Time

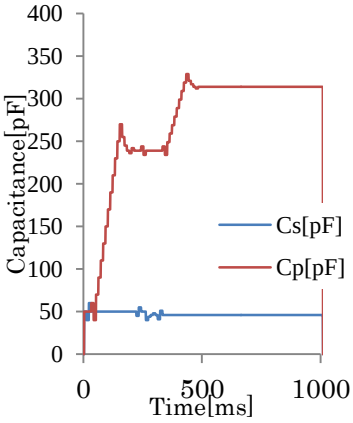

(ii) (C_s,C_p) vs Time GSS-Scalar

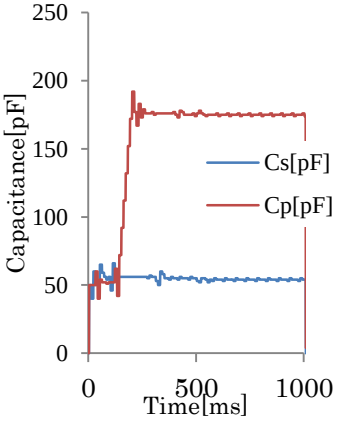

(iii) (C_s,C_p) vs Time GSS-Vector

(e) Gap = 18cm, L-matching circuit and L_s = 4μH

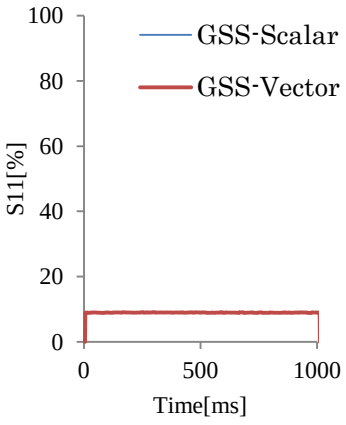

(i) S_{11} vs Time

(f) Gap = 21cm, Matching circuit bypassed (thru)

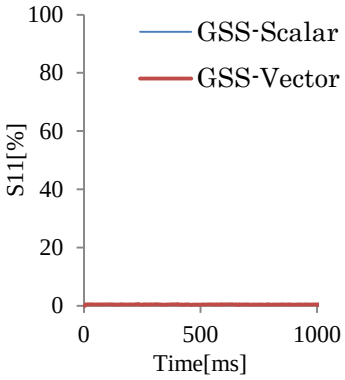

(i) S_{11} vs Time

(g) Gap = 24cm, Matching circuit bypassed (thru)

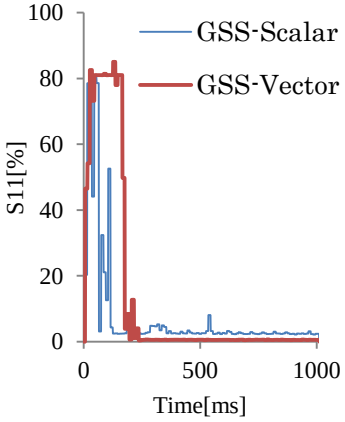

(i) S_{11} vs Time

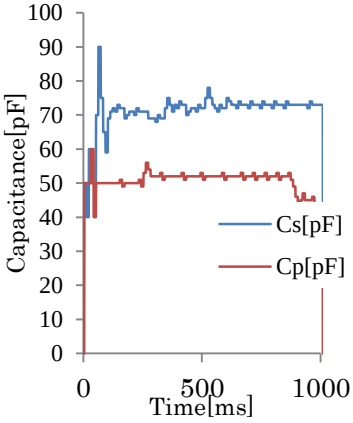

(ii) (C_s,C_p) vs Time
GSS-Scalar

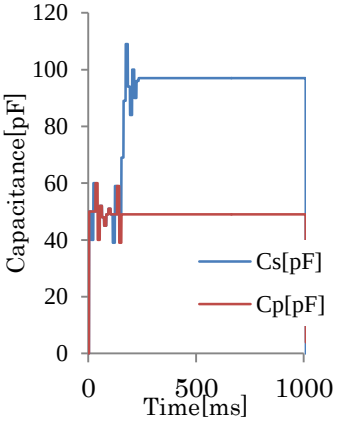

(iii) (C_s,C_p) vs Time
GSS-Vector

(h) Gap = 27cm, Inversed L-matching and L_s = 1.4μH

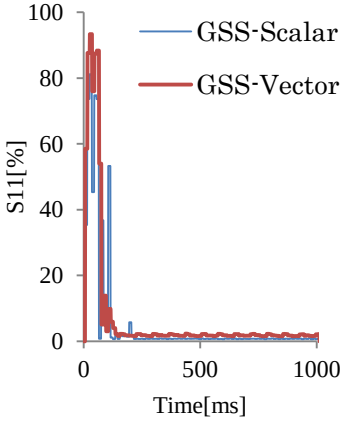

(i) S_{11} vs Time

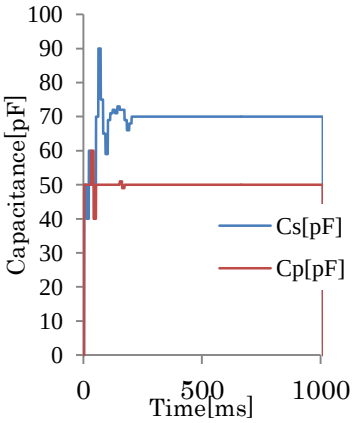

(ii) (C_s,C_p) vs Time
GSS-Scalar

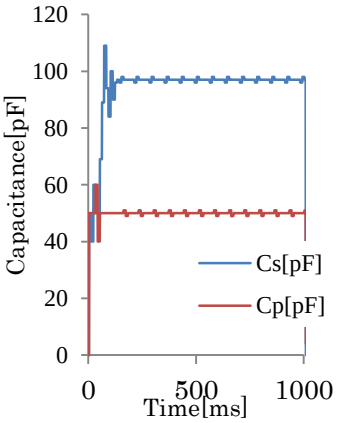

(iii) (C_s,C_p) vs Time
GSS-Vector

(i) Gap = 30cm, Inversed L-matching and L_s = 1.4μH

Fig 6.7. Experimental results of WPT with proposed automated IM system using GSS. Comparison of S_{11} and matching parameters vs time graphs of the GSS matching process. Matching topography and L_s is preselected for this experiment.

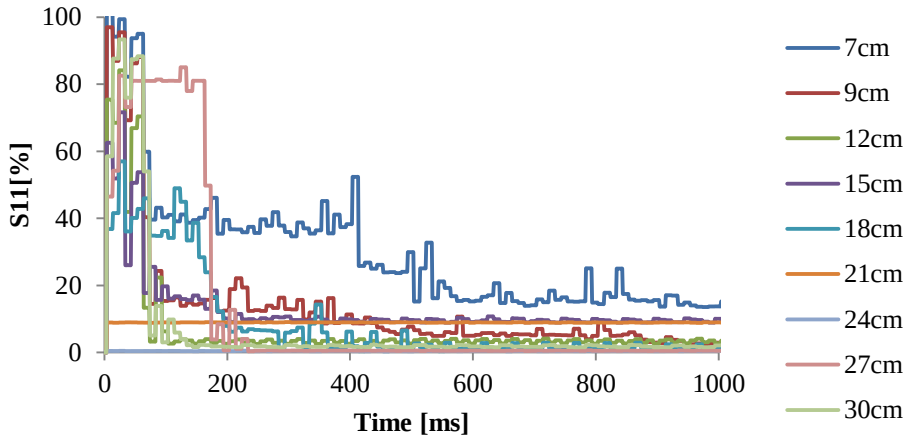

(a) GSS- Vector

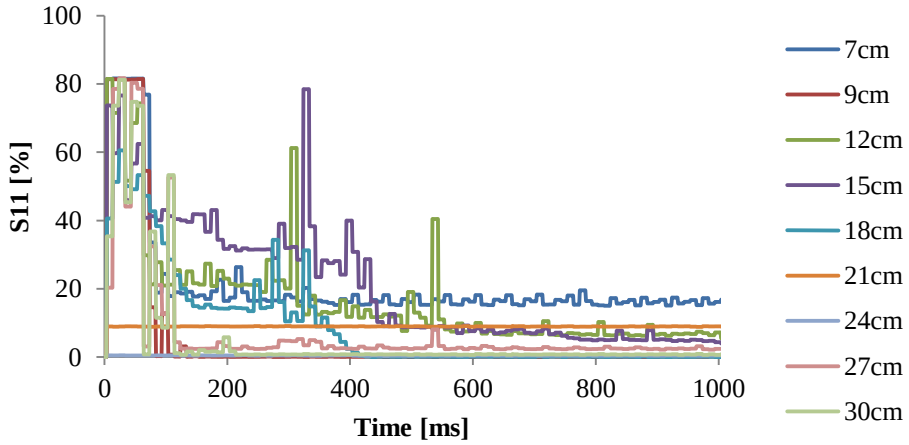

(b) GSS- Scalar

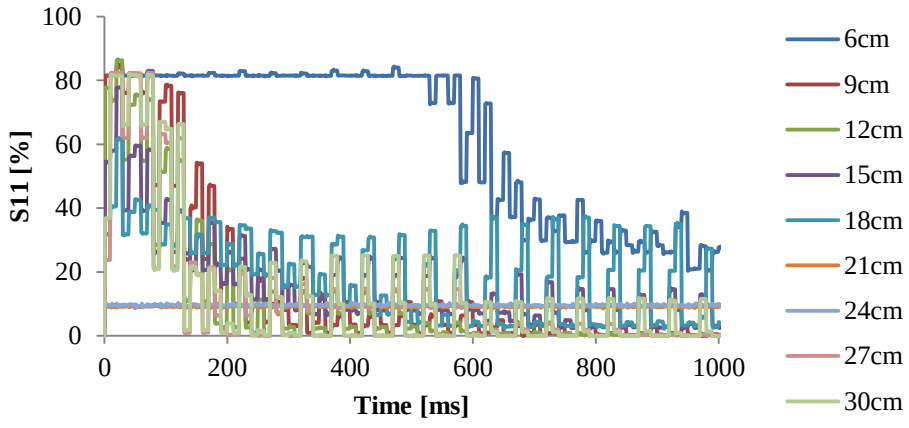

(c) BSSG (From Chapter 4)

Fig 6.8 S_{11} vs Time results comparison for different matching algorithms. (For time = 0s ~ 1s)

Fig 6.7 shows the detailed comparison of the S_{11} and matching parameter time response between the Scalar and Vector GSS. The graphs in Fig 6.8 are a comparison of the S_{11} time response for the Vector GSS, Scalar GSS and BSSG. The results in Fig 6.8 shows that the GSS greatly improves the matching time (the time it takes to stabilize below 20% reflection) of the system from 0.5s ~ 2.0s with the BSSG to 0.15s to 0.6s with the GSS. This matching speed can be considered the achievable matching time using the current industrial optimization methods. While more improvements can be made, (such as improving the β selection to make it expand exponentially at a ratio of the golden section, or linearizing the α and β selection according to the S_{11} instead of making it digital, and choosing a better starting parameter) the order of the matching time will probably not change, with only slight improvements to the matching time.

Although the Vector GSS should theoretically reach a slightly faster matching speed, there are no significant matching speed difference between the two GSS search algorithms. The main reason for that is because it is only a two dimensional problem, where the slight difference in ratio will not make such a significant difference. Vector GSS generally has a more stable response, with less small peaks which occur when the matching parameters move out of the low S_{11} area during the direction search phase. The effect of using the Vector GSS will be clearer only in high dimension problems, so that the difference between the number of iterations becomes bigger. In fact, from the simulation results in Fig 5.1, it can be said that for most cases, the major tuning can be done on C_s as it has the biggest impact on the S_{11} characteristics. This can be confirmed by looking at the Vector-GSS results of Fig 6.7(a)~(i), the bracketing and GSS loop mainly occurs only on one side at a time, with a very small change in the other parameter (approximately 10 times smaller than its counterpart)

Experiment on Moving Receiver

Finally, to test the potential of the proposed GSS algorithm on moving objects, the IM system was run real-time while the receiver is moving. Fig 6.9 shows the experimental setup for this experiment. The transmitter (left resonator) was fixed, and the receiver (right resonator) was moved towards the right of the picture from 8cm air gap (initial point), to 18cm air gap, and back again to 8cm after a pause. The experiment methodology goes as below

1. The initial air gap is fixed at 8cm.
2. The IM system is activated real time. The resonator pair are matched at 8cm gap.
3. The receiving resonator were moved from 8cm to 18cm by hand.
4. The receiving resonator is left at 18cm for a short while, before moving it back to 8cm.

Two cases were tested, one where the receiver was moved slowly (taking more than 1s) and one where the receiver was moved quickly (taking less than 1s) to see how well the resonators can be matched. Both the Scalar and Vector GSS were tested. The results for the slow moving case and fast moving case are shown in Fig 6.10 and Fig 6.11 respectively. Note that as the resonators were

manually moved by hand, the speed and time at which the resonators were moved were different. (the time at which the receiver were moved is written in the brackets). Therefore, this experiment is strictly for reference only, and the results do not show the actual comparison of the Scalar and Vector GSS matching potential. . While the low repeatability of the experiment makes it less scientific, the result gives us a good idea on how well the IM system can work in an actual moving object

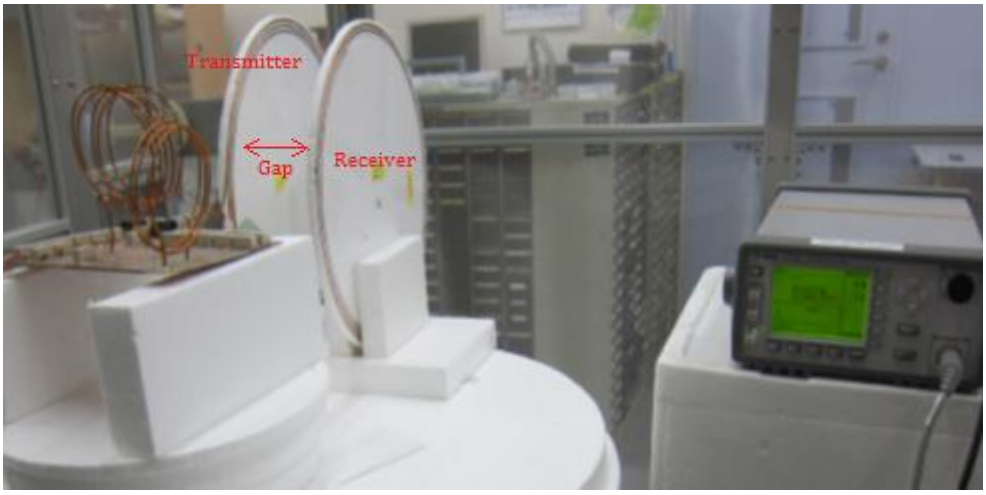

Fig 6.9 Photo of experiment for moving receiver.

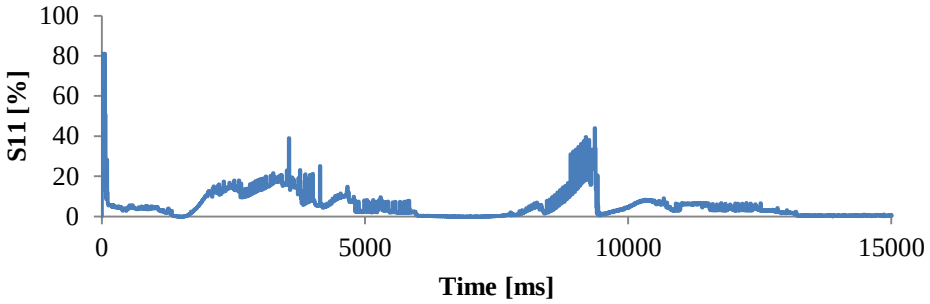

(a) Scalar (8cm→18cm at 1330ms ~ 6000ms) (18cm→8cm at 7500ms ~ 9400ms)

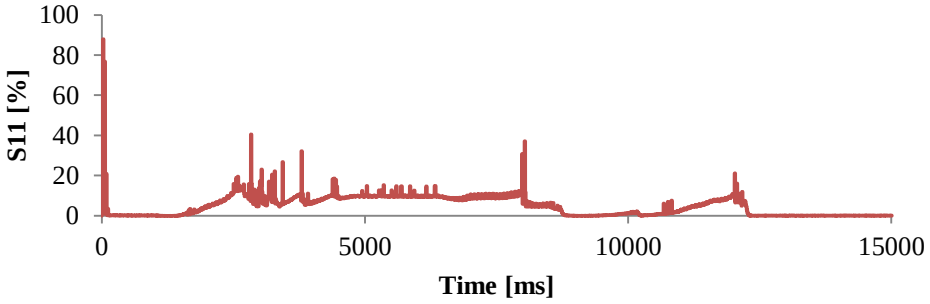

(b) Vector (8cm→18cm at 1400ms ~ 8500ms) (18cm→8cm at 10300ms ~ 12000ms)

Fig 6.10 S_{11} vs time graphs of experiment of slow moving receiver. (moves for longer than 1s) Receiver moves slowly with the course (8cm → 18cm → pause → 8cm)

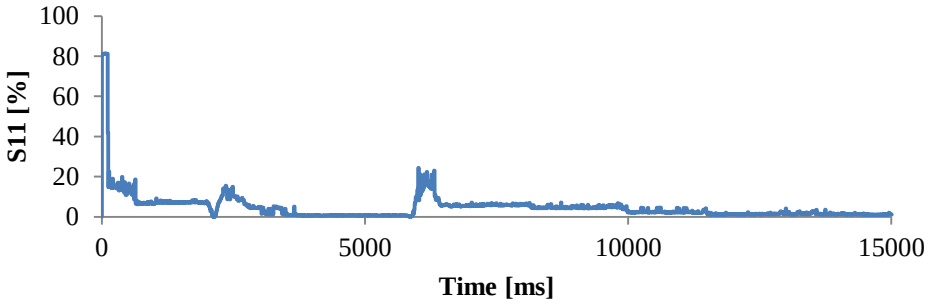

(a) Scalar (8cm→18cm at 2000ms ~ 3000ms) (18cm→8cm at 6000ms ~ 6300ms)

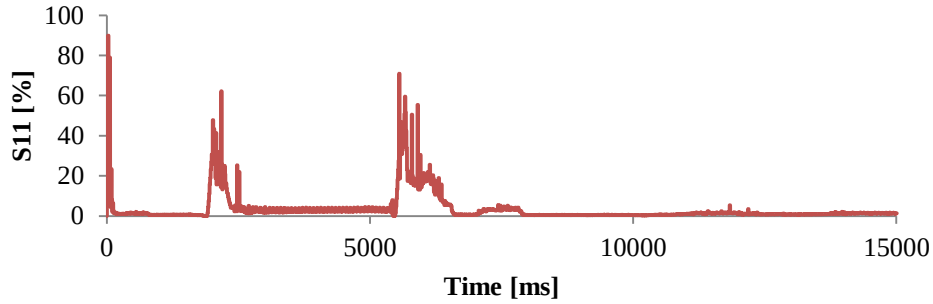

(b) Vector (8cm→18cm at 1600ms ~ 2300ms) (18cm→8cm at 5200ms ~ 6300ms)

Fig 6.11 S_{11} vs time graphs of experiment of fast moving receiver. (moves in 1s or less) Receiver moves almost instantaneously with the course (8cm → 18cm → pause → 8cm)

The experimental results show that the proposed IM system with GSS can maintain the S_{11} of the resonator pair below 40% generally, with occasional peaks at approximately 60%. This means that the efficiency can be maintained at a high efficiency most of the time. This result is important to show that the GSS still satisfy the second condition mentioned in Section 6.1, (the optimum point of $f(\boldsymbol{x})$ is located within an interval $\boldsymbol{x}_{\mathrm{gsmin}} \leqq \boldsymbol{x} \leqq \boldsymbol{x}_{\mathrm{gsmax}}$), even when the receiver is moving because the time taken to finish a loop of GSS is much smaller than the time it takes to significantly change the S_{11} characteristics of the resonator pair.

The reason the S_{11} peaks occur is probably due to the C_s parameter moving out of the narrow low S_{11} parts. This occurs at large air-gaps (as shown in Fig 5.1.), where the C_s parameter is particularly sensitive. As mentioned above, the low repeatability of the experiment (done by hand) does not allow us to compare the S_{11} characteristics between the two algorithms tested.

6.3 Summary and Future Work

As a conclusion, a two dimension optimization algorithm based on the Golden Section Search was proposed to automate the IM circuit to match the resonators in the MRC WPT system. The GSS was used to improve the matching time compared to the BSSG introduced in Chapter 5. The matching speed is vital for practical usage of the MRC system for cases such as a moving object or a varying load impedance. Two methods to determine the direction of which the GSS is conducted, namely the Scalar GSS and Vector GSS, were tested. The former uses the direction of the parameter with the

lowest S_{11} reading while the latter choose the direction in between the steepest direction for the series and parallel capacitor according to their respective ratio.

Experimental results show that the proposed GSS algorithm can improve the matching time to 0.15s ~ 0.6s (compared to 0.5s ~ 2s using BSSG). The experimental results for moving objects show that the GSS can maintain the S_{11} below 40% most of the time with occasional peaks at 60%, meaning a high efficiency can be maintained even for moving objects. The occasional peaks occur when the C_s parameter moves out of the narrow high efficiency zone when the air gap is far. The results also show that the method at which the direction is chosen to conduct GSS does not significantly affect the matching time and post-matched efficiency (80% to 85%). This is mainly due to the low number of parameters, which limits the advantage of the Vector based search direction.

The matching speed achieved in these experiments can be considered the achievable matching time using the current industrial optimization algorithms. The factors limiting the matching speed now can be considered hardware limits such as chattering time of the relays and the sampling number. While not expected to have a significant improvement in matching speed, there are several improvements that can still be made in the GSS search algorithm such as:

- Improving the direction search step size α and bracketing step size β by making it a function of S_{11} instead of pre-determined conditions.
- Improving the bracketing step size by making it expand exponentially larger according to the golden section ratio, starting from a smaller size. (currently bracketing process is swept at a constant step size)
- Choosing a better starting parameter

Furthermore, the matching speed can also be improved by including more measurements to get a better starting parameter. This can be done by measuring the voltage, current and phase at the transmitting side to calculate the total impedance of the system so an initial parameter closer to the peak can be selected. If the parameters of the resonators are known, estimation of the coupling factor k and load impedance Z_{load} will further improve the matching time by calculating the needed matching parameters based on the equivalent circuit.

Chapter7 Conclusion

As a conclusion, an automated IM system has been proposed to maintain the resonance of a MRC wireless power transfer system with a fixed frequency at 13.56MHz. The proposed IM system is explained in Chapter 3. The IM system uses a directional coupler to measure the reflected wave ratio at the transmitting end of the system, and high frequency relays were used to select the matching parameters needed to minimize the reflected wave.

- In Chapter 4, the effect of IM on MRC was tested with an IM circuit whose parameters are manually inserted. Experiment and simulation results show that the IM circuit increases the efficiency by matching the resonance frequency of the resonator to 13.56MHz, and extends the range of the wireless power transfer system by making a sharper peak at the resonance frequency.The efficiency can be increased to 85%, and the range at which the efficiency is above 70% is increased to 34cm (from approximately 25cm). The efficiency here can be considered the highest achievable with an IM circuit as of the 15% efficiency lost, 5% is due to the ohm loss and radiation loss of the resonators, and 10% is due to the ohm loss of the components of the IM circuit and the stray reactance of the IM circuit.
- In Chapter 5, the automation of the proposed IM system is verified. The simulation result of the characteristic of the efficiency versus the matching parameters shows that the efficiency has a single peak and a smooth gradient. Next, an experiment was done using the Best Step Steepest Gradient (BSSG) Method to minimize the reflected wave of the system. The efficiency can be increase to up to 85% (almost ideal) within 0.5s to 2s using this simple matching algorithm that is not optimized for speed. The results also validated that the automation can be conducted easily due to the single peak and smooth gradient of the efficiency characteristic. This means that the choice of matching algorithm is very wide, and there are many opportunities to improve the matching speed and precision of the IM system.
- Finally, in Chapter 6, the maximum achievable matching speed was studied using a proposed search algorithm that is based on the Golden Section Search (GSS) method. The experiment results show that the matching time can be decreased to 0.2s to 0.6s using the GSS search algorithm, an almost 100% improvement compared to the BSSG. The results also show that the matching speed and efficiency is not significantly affected by the vector direction at which the matching parameters are swept due to the small number of control parameters. The faster matching speed allows the WPT system to be more robust towards positional shifts and varying load, a vital factor in WPT for moving objects or systems with varying load impedances such as EDLC charging.This matching speed can be considered almost the achievable speed using this particular setup, with the hardware as the limiting factor (such as chattering time of the relays and sampling number). Further improvements can still be done to the matching algorithm such as choosing a better initial parameter, and better scaling of

the direction search loop and bracketing loop step size, such as scaling the bracketing loop step size exponentially with the golden section method.

Also, as a side topic for future experiments including varying loads, the definition of efficiency is studied in Chapter 2. The frequency characteristics and power transfer efficiency of MRC using equivalent circuits, electromagnetic analysis, simulations and experiments. The study was conducted to compare the definition of power transfer efficiency using S-parameters, and power electronics (voltage and current sensors).It shows that power reflection occurs at high frequency (13.56MHz), and it leads to a loss in power transfer efficiency. Therefore, when measuring efficiency with voltage and current sensors, the reflected wave must also be taken into consideration. The efficiency should be defined as the ratio of the active power reaching the load and the active power of the forward wave from the power source. This definition of efficiency agrees with the results of the S-parameters in both simulations and experiment.

Future Topics

The effect of IM on MRC, and the benchmark of the maximum efficiency and matching speed of the proposed IM system have been studied. However, to allow the MRC WPT to be practical, such as charging an EDLC on a moving vehicle, more improvements must be made. Possible future works include:

- Improve the search algorithm by choosing a better initial parameter, and by better scaling of the step sizes in the search loop. For example, the step size of the direction search loop can be scaled according to the wave reflection ratio. Moreover, the step size of the bracketing loop can be scaled exponentially according to the golden section method to potentially reduce the number of steps needed in the bracketing loop. Lastly, a completely new search algorithm can also be explored as the efficiency characteristic allows a wide range of options.
- Improving the matching speed by including voltage and current sensors at the transmitting end to measure the impedance of the system, and calculate an appropriate initial parameter. This will also allow the automatic selection of the matching topography, allowing the IM system to be even more adaptive to gap changes.While this will increase the matching speed, a search algorithm is still needed to improve the precision of the matching parameters. This is because the stray reactance of the IM circuit will affect the value of the parameters selected.
- Including a matching system on the receiver end to adapt to drastic changes in the impedance of the load. This is especially important for EDLC charging as the impedance of the super-capacitor changes drastically as the state-of-charge changes. This can be done by using other matching systems such as a dc/dc converter after the wave is rectified to maintain the impedance of the load.

- Estimate the parameters of the WPT system such as the coupling factor and load impedance so that a suitable matching parameter can be instantly chosen both for increasing efficiency and power distribution to multiple loads.
- Conduct the IM experiments for varying load. These experiments can be conducted to see the matching speed needed to adapt to changing load impedances such as the EDLC.
- Explore other options of the hardware of IM circuit, such as using a hybrid of motor controlled variable capacitors, and relay controlled ceramic condensers. Including a variable capacitor as a "rough tuning parameter" will reduce the number of ceramic condensers needed. This will lead to a smaller matching circuit, which is not only cheaper and more convenient, but also potentially less prone to stray reactance.
- Expand the study on the definition of efficiency to lower frequencies such as the kHz range, where the reflection has less effect on the efficiency, and the standing wave does not occur. Also, the limit at which the power reflection should be considered an efficiency loss should also be studied.

Towards Charging of Moving Objects

To perform high efficiency wireless charging of EVs, it is needless to say that a fast matching speed is needed. However, there are other factors too, such as the speed of the moving car, and the size of the transmitting resonator. Therefore, while a 0.15s ~ 0.6s matching time might not suffice for an EV that is moving at 100kmph, we can solve this problem by making a much larger transmitting resonator. For example, by stretching the size of each the transmitting resonator to up to 50m (or even 100m to 1km, depending on the requirements) or so, which is quite reasonable as this will mean less power sources will be needed in the charging lane, the change in coupling factor will be less while the EV is within the area of the resonator. This will mean that the impedance will change less during this period, which gives the matching system ample time to reach a high efficiency. The relation of resonator size, receiver moving speed and matching time is an interesting future topic in my opinion.

Acknowledgement

First of all, I would like to thank Professor Yoichi Hori, Professor Hiroshi Fujimoto and Dr. Takehiro Imura for the two to three years of guidance, support, trust and opportunity offered.

Special thanks to Masaki Kato for the technical guidance in making the experimental setup, and the rest of the WPT team (Moriwaki, Palakon, Koh, Paopao and Tsuboka) for the advice and assistance that greatly contributed to my research, and for the cooperation in the demanding but highly motivating team projects. Same goes to Dr. Sehoon Oh and the Welfare-Robotics team (particularly Dr. Valerio, Kimura, Kayoung, Koji and Sonokawa) for the help in setting up the computer used in the experiment, and for generously sharing their computer when the original one broke down.

Last but not the least, a big thanks to the members of the Hori-Fujimoto Laboratory and its associates especially Nam, Minaki, Alex and Zhu for the advice and support that greatly helped in everything from research to lab and personal life. My best wishes goes to the future undertakings of the laboratory. Thank you.

Reference

[1] Zhen Ning Low; Chinga, R.A.; Tseng, R.; Jenshan Lin; , "Design and Test of a High-Power High-Efficiency Loosely Coupled Planar Wireless Power Transfer System," *Industrial Electronics, IEEE Transactions on* , vol.56, no.5, pp.1801-1812, May 2009.

[2] Hirai, J.; Tae-Woong Kim; Kawamura, A.; , "Study on intelligent battery charging using inductive transmission of power and information," *Power Electronics, IEEE Transactions on* , vol.15, no.2, pp.335-345, Mar 2000

[3] Chang-Gyun Kim; Dong-Hyun Seo; Jung-Sik You; Jong-Hu Park; Cho, B.H.; , "Design of a contactless battery charger for cellular phone," *Industrial Electronics, IEEE Transactions on* , vol.48, no.6, pp.1238-1247, Dec 2001

[4] Jabbar, H.; Song, Y.S.; Jeong, T.T.; , "RF energy harvesting system and circuits for charging of mobile devices," *Consumer Electronics, IEEE Transactions on* , vol.56, no.1, pp.247-253, February 2010

[5] Sai Chun Tang; Jolesz, F.A.; Clement, G.T.; , "A wireless batteryless deep-seated implantable ultrasonic pulser-receiver powered by magnetic coupling," *Ultrasonics, Ferroelectrics and Frequency Control, IEEE Transactions on* , vol.58, no.6, pp.1211-1221, June 2011

[6] Shiba, K.; Morimasa, A.; Hirano, H.; , "Design and Development of Low-Loss Transformer for Powering Small Implantable Medical Devices," *Biomedical Circuits and Systems, IEEE Transactions on* , vol.4, no.2, pp.77-85, April 2010

[7] Fei Zhang; Xiaoyu Liu; Hackworth, S.A.; Sclabassi, R.J.; Mingui Sun; , "In vitro and in vivo studies on wireless powering of medical sensors and implantable devices," *Life Science Systems and Applications Workshop, 2009. LiSSA 2009. IEEE/NIH* , vol., no., pp.84-87, 9-10 April 2009

[8] Madawala, U.K.; Thrimawithana, D.J.; , "A Bidirectional Inductive Power Interface for Electric Vehicles in V2G Systems," *Industrial Electronics, IEEE Transactions on* , vol.58, no.10, pp.4789-4796, Oct. 2011

[9] Chwei-Sen Wang; Stielau, O.H.; Covic, G.A.; , "Design considerations for a contactless electric vehicle battery charger," *Industrial Electronics, IEEE Transactions on* , vol.52, no.5, pp. 1308- 1314, Oct. 2005

[10] A. Karalis , J. D. Joannopoulos and M. Soljai "Efficient wireless non-radiative mid-range energy transfer", *Ann. Phys.*, vol. 323, no. 1, pp.34 -48 2008

[11] A. Kurs , A. Karalis , R. Moffatt , J. D. Joannopoulos , P. Fisher and M. Soljai "Wireless power transfer via strongly coupled magnetic resonances", *Sci. Exp.*, vol. 317, no. 5834, pp.83 -86 2007

[12] N. Tesla, "Apparatus for transmission of electrical energy," U.S. Patent 649, 621, dated May 15, 1900.

[13] Ho, S.L.; Junhua Wang; Fu, W.N.; Mingui Sun; , "A Comparative Study Between Novel Witricity and Traditional Inductive Magnetic Coupling in Wireless Charging," *Magnetics, IEEE Transactions on* , vol.47, no.5, pp.1522-1525, May 2011

[14] Mur-Miranda, J.O.; Fanti, G.; Yifei Feng; Omanakuttan, K.; Ongie, R.; Setjoadi, A.; Sharpe, N.; , "Wireless power transfer using weakly coupled magnetostatic resonators," *Energy Conversion Congress and Exposition (ECCE), 2010 IEEE* , vol., no., pp.4179-4186, 12-16 Sept. 2010

[15] Sanghoon Cheon; Yong-Hae Kim; Seung-Youl Kang; Myung Lae Lee; Jong-Moo Lee; Taehyoung Zyung; , "Circuit-Model-Based Analysis of a Wireless Energy-Transfer System via Coupled Magnetic Resonances," *Industrial Electronics, IEEE Transactions on* , vol.58, no.7, pp.2906-2914, July 2011

[16] Imura, T.; Hori, Y.; , "Maximizing Air Gap and Efficiency of Magnetic Resonant Coupling for Wireless Power Transfer Using Equivalent Circuit and Neumann Formula," *Industrial Electronics, IEEE Transactions on* , vol.58, no.10, pp.4746-4752, Oct. 2011

[17] Imura, T.; Okabe, H.; Uchida, T.; Hori, Y.; , "Study on open and short end helical antennas with capacitor in series of wireless power transfer using magnetic resonant couplings," *Industrial Electronics, 2009. IECON '09. 35th Annual Conference of IEEE* , vol., no., pp.3848-3853, 3-5 Nov. 2009

[18] Imura, T.; Okabe, H.; Uchida, T.; Hori, Y.; , "Study on open and short end helical antennas with capacitor in series of wireless power transfer using magnetic resonant couplings," *Industrial Electronics, 2009. IECON '09. 35th Annual Conference of IEEE* , vol., no., pp.3848-3853, 3-5 Nov. 2009

[19] T.C. Beh, M. Kato, T. Imura, Y. Hori, “Wireless Power Transfer System via Magnetic Resonant Coupling at Fixed Resonance Frequency –Power Transfer System Based on Impedance Matching–”, in *Proc. The 25th World Battery, Hybrid and Fuel Cell Electric Vehicle Symposium & Exhibition (EVS25),* 2010

[20] Teck Chuan Beh; Imura, T.; Kato, M.; Hori, Y.; , "Basic study of improving efficiency of wireless power transfer via magnetic resonance coupling based on impedance matching," *Industrial Electronics (ISIE), 2010 IEEE International Symposium on* , vol., no., pp.2011-2016, 4-7 July 2010

[21] Sample, A.P.; Meyer, D.A.; Smith, J.R.; , "Analysis, Experimental Results, and Range Adaptation of Magnetically Coupled Resonators for Wireless Power Transfer," *Industrial Electronics, IEEE Transactions on* , vol.58, no.2, pp.544-554, Feb. 2011

[22] Thuc Phi Duong; Jong-Wook Lee; , "Experimental Results of High-Efficiency Resonant Coupling Wireless Power Transfer Using a Variable Coupling Method," *Microwave and Wireless Components Letters, IEEE* , vol.21, no.8, pp.442-444, Aug. 2011

[23] Awai, I.; Komori, T.; , "A Simple and versatile design method of resonator-coupled wireless power transfer system," *Communications, Circuits and Systems (ICCCAS), 2010 International Conference on* , vol., no., pp.616-620, 28-30 July 2010

[24] van Bezooijen, A.; de Jongh, M.A.; van Straten, F.; Mahmoudi, R.; van Roermund, A.; , "Adaptive Impedance-Matching Techniques for Controlling L Networks," *Circuits and Systems I: Regular Papers, IEEE Transactions on* , vol.57, no.2, pp.495-505, Feb. 2010

[25] Arroyo-Huerta, E.; Diaz-Mendez, A.; Ramirez-Cortes, J.M.; Garcia, J.C.S.; , "An adaptive impedance matching approach based on fuzzy control," *Circuits and Systems, 2009. MWSCAS '09. 52nd IEEE International Midwest Symposium on* , vol., no., pp.889-892, 2-5 Aug. 2009

[26] Hirose, Y.; Kawamura, A.; Takayanagi, A.; Takada, H.; , "Analysis of impedance matching control," *Power Electronics and Motion Control Conference, 2009. IPEMC '09. IEEE 6th International* , vol., no., pp.1188-1191, 17-20 May 2009

[27] Cao-Minh Ta; Hori, Y.;, "Convergence improvement of efficiency-optimization control of induction motor drives," *Industry Applications, IEEE Transactions on* , vol.37, no.6, pp.1746-1753, Nov/Dec 2001

[28] TeckChuan Beh, Masaki Kato, Takehiro Imura, Yoichi Hori, "Wireless Power Transfer System via Magnetic Resonant Coupling at Restricted Frequency Range –Fixing Resonance Frequency With Impedance Matching-", *JIASC*, pp II 263 – II 266, 2010

[29] Prof. Dr. Thomas C. Baier, "A Simple S-Parameter Test Set for the VNWA2 Vector Network Analyzer", QEX – May/June 2009. Pg19-32

[30] K. Kurokawa, "Power Waves and the Scattering Matrix," *IEEE Trans. MTT*, vol. 13, no.3, pp. 196-202, March 1965

[31] Jussi Rahola, "Power Waves and Conjugate Matching" *IEEE Trans on Circuit and Systems- II: Express Briefs*, vol. 55, no. 1, January 2008

[32] TeckChuan Beh, "Basic Research on Wireless Power Transfer System via Magnetic Resonance Coupling at MHz Range – Efficiency Improvement Based on Impedance Matching- ", *Undergraduate Thesis, Department of Electrical and Electronic Engineering, University of Tokyo*, March 2010.

[33] Donald A.Pierre, "*Optimization Theory with Application*", Dover Publications, INC., New York, 1986

Publications

Transactions

[1] TeckChuan Beh, Masaki Kato, Sehoon Oh, Takehiro Imura, Yoichi Hori, "Automated Impedance Matching System for Robust Wireless Power Transfer via Magnetic Resonance Coupling", *Industrial Electronics, IEEE Transactions on* , (Under Review, Submitted Nov 2011)

[2] T.C. Beh, M. Kato, T. Imura, Y. Hori, "Wireless Power Transfer System via Magnetic Resonant Coupling at Fixed Resonance Frequency –Power Transfer System Based on Impedance Matching–",World Electric Vehicle Journal (WEVA Journal from EVS 25 proceeding), (Awaiting Reply, Invited Dec 2011)

International Conferences

[1] T.C. Beh, M. Kato, T. Imura, Y. Hori, "Wireless Power Transfer System via Magnetic Resonant Coupling at Fixed Resonance Frequency –Power Transfer System Based on Impedance Matching–", in *Proc. The 25th World Battery, Hybrid and Fuel Cell Electric Vehicle Symposium & Exhibition (EVS25),* 2010

[2] Teck Chuan Beh; Imura, T.; Kato, M.; Hori, Y.; , "Basic study of improving efficiency of wireless power transfer via magnetic resonance coupling based on impedance matching," *Industrial Electronics (ISIE), 2010 IEEE International Symposium on* , vol., no., pp.2011-2016, 4-7 July 2010

Local Conferences

[1] TeckChuan Beh, Masaki Kato, Takehiro Imura, Yoichi Hori, "Wireless Power Transfer System via Magnetic Resonant Coupling at Restricted Frequency Range –Fixing Resonance Frequency With Impedance Matching-", *JIASC,* pp II 263 – II 266, 2010